Electronic version of an article published as International Journal of Structural Stability and Dynamics, Vol. 20, No. 03, 2050039 (2020). https://doi.org/10.1142/S021945542050039X. © World Scientific Publishing Company. https://www.worldscientific.com/worldscinet/ijssd.

# A DSC Regularized Dirac-delta Method for Flexural Vibration of Elastically Supported FG Beams Subjected to a Moving Load

**L.H. Zhang**[a], **S.K. Lai**[a,b,*] and **J. Yang**[c]

[a] *Department of Civil and Environmental Engineering, The Hong Kong Polytechnic University, Kowloon, Hong Kong, P.R. China*

[b] *Hong Kong Branch of National Rail Transit Electrification and Automation Engineering Technology Research Center, The Hong Kong Polytechnic University, Kowloon, Hung Hom, Hong Kong, P.R. China*

[c] *School of Engineering, RMIT University, PO Box 71, Bundoora, VIC 3083, Australia*

## Abstract

This research presents a numerical approach to address the moving load problem of functionally graded (FG) beams with rotational elastic edge constraints, in which the regularized Dirac-delta function is used to describe a time-dependent moving load source. The governing partial differential equations of the system, derived in accordance with the classical Euler-Bernoulli beam theory, are approximated by the discrete singular convolution (DSC) method. The resulting set of algebraic equations can then be solved by the Newmark-$\beta$ integration scheme. Such a singular Dirac-delta formulation is also employed as the kernel function of the DSC method. In this work, the material properties of FG beams are assumed to be changed in the thickness direction. A convergence study is performed to validate the accuracy and reliability of the numerical results. In addition, the effects of moving load velocity and material

[*]Corresponding author. E-mail address: sk.lai@polyu.edu.hk

distribution on the dynamic behavior of elastically restrained FG beams are also studied to serve as new benchmark solutions. By comparing with the available results in the existing literature, the present results show good agreement. More importantly, the major finding of this work indicates that the DSC regularized Dirac-delta approach is a good candidate for moving load problems, since the equally spaced grid system adopted in the DSC scheme can achieve a preferable representation of moving load sources.

**Keywords**: Moving loads, Functionally graded beams, Elastic restraint, Dirac-delta function, DSC method.

## 1. Introduction

A vast number of studies on the dynamic behavior of beam-like structures subjected to a moving load have enjoyed thriving developments over the past few decades. This class of problems is of paramount significance due to their applications in a wide range of engineering fields. One practical example is to model as an ideal and simple structure of railway tracks/bridges that can be used to investigate the vehicle-track-bridge interaction. An illustrative application was presented by Madrazo-Aguirre et al. [1] who investigated the dynamic characteristics of steel-concrete composites under-deck cable-stayed bridges subjected to the action of moving loads. Konstantakopoulos et al. [2] developed a three-dimensional model of suspended bridges to demonstrate its dynamic performance under the impact of moving loads and seismic effects. Yau et al. [3] carried out a numerical assessment for the vehicle-bridge interaction of short-span railway bridges by using a constant moving load model. These analysis results are very important to establish or improve the design guidance for practitioners and engineers. With the advancement of modern railway transport infrastructure, there is still a growing and practical demand in this research area [4].

Many researchers have attempted to pursue accurate solutions for moving load problems by analytical or numerical approaches. Building on earlier efforts, Frýba [5] conducted a comprehensive study for the vibration of solid structures under a moving load. Meirovitch [6] provided analytical solutions for the dynamic response of beams subjected to a traveling force. It is well known that the dynamic displacement and stress behavior due to a moving load are significantly larger than those induced by the static ones [7]. In addition, an applied load moving its geometric point on beam structures in a time-dependent manner can increase the complexity of such problems. For this type of problem, Rieker et al. [8] investigated the relationship between the model accuracy and the number of elements employed to discretize a structure for moving load analysis. They suggested that the number of grid points should be at least two to eight times larger than that used for static analysis. By using the Lagrange equation, Kocatürk and Şimşek [9] studied the dynamic behavior of eccentrically pre-stressed viscoelastic Timoshenko beams subjected to a traveling harmonic load. Yang et al. [10] investigated the crack effect on an inhomogeneous beam under free and forced vibration motions. Kim [11, 12] presented the dynamic displacement response of an infinite Rayleigh beam-column and an axially loaded beam resting on an elastic foundation when the system is excited by a moving load. Corrêa et al. [13] further evaluated the influence of frictional dissipation on the displacement and bending moment dynamic amplifications for Euler-Bernoulli beams resting on a Winkler-type foundation. In addition, Aied and González [14] considered the velocity and magnitude of moving loads on the displacement and strain responses of simply supported beams. Svedholm et al. [15] provided an analytical solution for evaluating the dynamic response of non-proportionally damped beams subjected to a moving load. More recently, Yang and Wang [16] further presented the dynamic and stability responses of an inclined Euler beam under a vertical moving load. For more relevant research studies, readers may refer to a review study conducted by Ouyang [17].

Functionally graded materials (FGMs) are inhomogeneous composites that have gained considerable popularities due to their superior mechanical and thermal properties. The concept was first introduced by a group of Japanese scientists as a thermal barrier in 1980s [18, 19]. FGMs are usually made up of two (or more) layers with a continuous variation of material properties along a spatial direction, where the metal/alloy layer can strengthen mechanical performance and the ceramic layer can provide better thermal resistance. Because of its intrinsic properties, this leads to the reduction of stress concentration and thermal stress in contrast to conventional laminated composites. Practical areas of FGMs can be found in structural engineering, aerospace engineering and automotive manufacturing.

The existing work mainly focused on the static, buckling and free vibration analysis of FG beams [20-23], but there were few research studies on the forced vibration analysis of FG beams due to a moving load. In the literature, Yang et al. [10] employed a modal expansion technique to conduct the forced vibration analysis of cracked FG beams due to both axial and moving forces, in which the material properties of the beam were assumed to change exponentially along the thickness direction. The research work conducted by Simsek and Kocatürk [24] was probably the first attempt to consider a concentrated harmonic load moving on a FG beam. After that, Simsek and his co-workers [25-27] contributed great efforts to investigate the dynamic characteristics of FG beams under a moving load using different beam theories. On the other hand, Khalili et al. [28] developed a mixed Ritz-DQ method for the moving load problem of FG beams. In their work, the differential quadrature method (DQM) was an efficient way for the discretization of temporal derivatives. Based on the classical and Timoshenko beam theories, Wang and Wu [29] further investigated the thermal effect on the dynamic characteristics of axially FG beams under a moving load. Nguyen et al. [30] used Hamilton's principle to construct the equations of motion for studying the vibration of bi-dimensional FG beams excited by a constant moving load. Songsuwan et al. [31] adopted the Ritz method to investigate the free and forced dynamic responses of FG sandwich beams resting on an elastic foundation under the action of a moving harmonic load. More recently, Yang et al. [32] presented new results for the dynamic performance of tapered bi-direction FG beams due to a moving harmonic load, in which the effects of taper ratio, material gradient, boundary condition, and moving speed on the vibration behavior were discussed.

In general, a point load moving on a beam structure can be represented by the Dirac-delta function. Due to the special characteristics of this time-dependent singular function, it is hard to directly apply strong-form based methods and there are very limited research studies for this problem. Illustrative examples can be referred to some hybridized numerical techniques. For example, Khalili et al. [28] exploited a mixed Ritz-DQ method for the moving load problem, wherein the weak-form based Rayleigh-Ritz method showed good simplicity by directly integrating the governing equations with the Dirac-delta function and the DQM for the discretization of time derivatives. After that, Jafari and Eftekhari [33] further proposed a numerical finite element-DQ formulation for this class of time-dependent problems. In addition, Wang and Jin [34] applied the modified DQM version to deal with the vibration problem of a moving load beam-type problem.

From a computational point of view, a moving concentrated point can be allocated to all grid points by the work-equivalent principle to circumvent the dimensional inconsistency between the system matrices and the load vectors. Based on this, Wang et al. [35] proposed an N-node weak form quadrature beam element to analyze the dynamic behavior of the FG beams carrying a moving load. Song et al. [36] adopted a frequency-domain spectral element method to investigate the dynamic performance of a beam under the effect of a moving load. They considered the moving load as the superposition of a series of stationary point forces, and the dynamic deflection of each grid point can be obtained accordingly. Recently, Eftekhari [37] further investigated the applicability of using the regularized Dirac-delta function for a time-dependent traveling load problem. With the implementation of this special treatment, the DQ procedures can be easily applied for the moving load problem of beams and plates. Indeed, the regularized Dirac-delta function is a suitable and simple manner for the representation of moving loads.

In fact, delta-type functions have been successfully applied as a kernel function to formulate an effective numerical algorithm that is known as the discrete singular convolution (DSC) method. Due to the special features of the singular delta function, this unified numerical method provides better stability and higher accuracy in the prediction of thousands of vibration modes of beams and plates as compared to DQM [38, 39]. On the other hand, evenly spaced grid points in terms of the DSC method for treating spatial differential equations can readily accommodate the approximation of moving loads using the regularized Dirac-delta function.

The DSC method is based on the theory of distribution and wavelet analysis, which was originally introduced by Wei [40, 41] for solving the Fokker-Planck equation. This method possesses good accuracy and stability for solving complex geometries and boundary conditions due to its local-spectral nature [42]. Making use of the DSC method, Lai and Xiang [43] conducted the buckling and vibration analysis of rectangular plates under linearly varying in-plane loads. To release the limitations of DSC, Wang et al. [44, 45] incorporated the Taylor series expansion method to handle the structural problems with free boundaries. In addition, Gao et al. [46] introduced a hybridized computational CSM-DSC approach to study the nondeterministic dynamic behavior of FG porous beams with material uncertainties. More recently, Kara and Seçgin [47] also improved the DSC approach for the vibro-acoustic analysis of structures having complex impedance boundary constraints.

The present study is the first attempt to put forward the application of the DSC method on moving load problems of elastically supported FG beams. It is found that the regularized Dirac-delta function plays a pivotal role in the DSC method to approximate moving load sources. In this work, two levels of discretization (i.e., spatial and temporal) are involved: the DSC regularized Dirac-delta approach is employed to approximate the governing equations, and the Newmark-$\beta$ integration scheme [48] is used to discretize the time derivatives.

## 2. Properties of Functionally Graded Materials

Consider an elastically restrained functionally graded (FG) beam with a span length $L$, width $b$, and thickness $h$. The coordinate system is shown in Fig. 1. The FG beam is subjected to a concentrated moving load $P(t)$, which moves along the axial direction with a constant velocity $v$. This moving load enters the beam at $t = 0$ and leaves at $t = v/L$.

In this study, it is assumed that ceramic and metal are used to constitute the FG beam. The effective material properties, including elasticity modulus $E$ and mass density $\rho$, are supposed to vary smoothly and continuously in the thickness direction based on the following power-law functions

$$\begin{aligned} E(z) &= (E_t - E_b)\left(\frac{z}{h} + \frac{1}{2}\right)^k + E_b \\ \rho(z) &= (\rho_t - \rho_b)\left(\frac{z}{h} + \frac{1}{2}\right)^k + \rho_b \end{aligned} \tag{1}$$

or the exponential distributions

$$\begin{aligned} E(z) &= E_t \exp[-\delta_E(1 - 2z/h)], \quad \delta_E = \frac{1}{2}\log\left(\frac{E_t}{E_b}\right) \\ \rho(z) &= \rho_t \exp[-\delta_D(1 - 2z/h)], \quad \delta_D = \frac{1}{2}\log\left(\frac{\rho_t}{\rho_b}\right) \end{aligned} \tag{2}$$

where the subscripts $t$ and $b$ are the corresponding material properties at the top surface ($z = h/2$) and the bottom surface ($z = -h/2$) of the FG beam, respectively. It is noted that the positive real number $k$ $(0 \le k \le \infty)$ in the power-law functions relates to the material variation profile through the thickness, as shown in Fig. 2.

## 3. Problem Formulation

### *3.1. Governing equations of FG beams subjected to a moving load*

Based on the Euler-Bernoulli beam theory, the axial displacement and transverse deflection of a beam can be expressed as [49]

$$u(x,z,t) = u_0(x,t) - z\frac{\partial w_0(x,t)}{\partial x},\qquad w(x,z,t) = w_0(x,t) \tag{3}$$

where $u_0(x,t)$ and $w_0(x,t)$ are the displacements at the mid-plane. According to the elastic constitutive law, one can obtain the strain-displacement relationship ($\varepsilon_{xx}$) and normal stress ($\sigma_{xx}$) of the beam as follows

$$\varepsilon_{xx} = \frac{\partial u_0}{\partial x} - z\frac{\partial^2 w_0}{\partial x^2} \tag{4}$$

$$\sigma_{xx} = E(z)\left(\frac{\partial u_0}{\partial x} - z\frac{\partial^2 w_0}{\partial x^2}\right) \tag{5}$$

Then, the normal force resultant ($N_x$) and moment resultant ($M_x$) at the cross-section of the beam can be expressed as

$$N_x = \int_A \sigma_{xx} dA = A_{11}\frac{\partial u_0}{\partial x} - B_{11}\frac{\partial^2 w_0}{\partial x^2} \tag{6}$$

$$M_x = \int_A \sigma_{xx} z dA = B_{11}\frac{\partial u_0}{\partial x} - D_{11}\frac{\partial^2 w_0}{\partial x^2} \tag{7}$$

where the extensional stiffness ($A_{11}$), extensional-bending coupling stiffness ($B_{11}$), and bending stiffness ($D_{11}$) of the FG beam can be calculated by

$$(A_{11}, B_{11}, D_{11}) = \int_{-h/2}^{h/2}\int_{-b/2}^{b/2} E(z)(1, z, z^2) dy\, dz \tag{8}$$

Consider a small element of the beam and assume that the axial inertia is neglected, the dynamic governing equation of the beam can be derived through the balance forces on the element ($\partial N_x/\partial x = 0, \partial M_x/\partial x - I_0(\partial^2 w_0/\partial t^2) = Q$) as

$$A_{11}\frac{\partial^2 u_0(x,t)}{\partial x^2} - B_{11}\frac{\partial^3 w_0(x,t)}{\partial x^3} = 0 \tag{9}$$

$$B_{11}\frac{\partial^3 u_0(x,t)}{\partial x^3} - D_{11}\frac{\partial^4 w_0(x,t)}{\partial x^4} - I_0\frac{\partial^2 w_0(x,t)}{\partial t^2} = Q \tag{10}$$

where $I_0 = \int_{-h/2}^{h/2}\int_{-b/2}^{b/2}\rho(z)dy\,dz$ is the inertia moment of the FG beam, and $Q$ is the transverse force applying on the beam. Taking the moving load into account, the equations of motion can be further reduced to the following form

$$\left(D_{11} - \frac{B_{11}^2}{A_{11}}\right)\frac{\partial^4 w_0(x,t)}{\partial x^4} + I_0\frac{\partial^2 w_0(x,t)}{\partial t^2} = P(t) \tag{11}$$

where $w_0(x,t)$ is the lateral deflection, $P(t) = -f\delta(x - x_p(t))$ is the moving load, $\delta(\cdot)$ represents the Dirac-delta function, and $x_p(t) = v_p t$ is the position coordinate of the moving load.

*3.2.Regularization of the Dirac-delta function*

Due to the particular properties of the Dirac-delta function, it is difficult to directly apply the discretization of grid points, such as the collocation method and the finite element method for handling moving load problems. In this regard, the regularized form of singular functions with good smoothness and stability becomes a good candidate. In the literature, various types of approximated Dirac-delta functions have been proposed. For example, the Gauss' delta function is expressed as [50]

$$\delta(x) = \frac{1}{\sqrt{2\pi}\varepsilon}\exp\left(-\frac{x^2}{2\varepsilon^2}\right) \quad for\ \varepsilon \to 0 \tag{12}$$

where $\varepsilon$ is the parameter to control the smoothness and accuracy of approximations. The dimensionless discretized form can be expressed as

$$\delta(\xi-\xi_0)\approx\frac{1}{\sqrt{2\pi}\varepsilon}\exp\left[-\frac{(\xi-\xi_0)^2}{2\varepsilon^2}\right]\quad for\ \varepsilon\to 0 \tag{13}$$

where $0\leq\xi\leq 1$. By introducing the following dimensionless parameters

$$\xi=\frac{x}{L},\quad W_0=\frac{w_0}{L},\quad \xi_p(t)=\frac{x_p(t)}{L}=\frac{vt}{L} \tag{14}$$

Making use of Eqs. (11), (13) and (14) yields

$$\left(D_{11}-\frac{B_{11}^2}{A_{11}}\right)\frac{\partial^4 W_0(\xi,t)}{\partial\xi^4}+I_0L^4\frac{\partial^2 W_0(\xi,t)}{\partial t^2}=-\frac{fL^3}{\sqrt{2\pi}\varepsilon}\exp\left[-\frac{\left(\xi-\xi_p(t)\right)^2}{2\varepsilon^2}\right] \tag{15}$$

According to Eq. (13), it is easy to imagine that the discretized model with a large number of grid points and a small value of $\varepsilon$ can provide a better representation of the original continuous model. For comparison, we define the regularized parameter as $\alpha=\sqrt{2}\varepsilon$. Eftekhari [37] demonstrated some numerical applications of the regularized Dirac-delta function for moving load problems. In the work, the use of DQM for the approximation of transverse deflection $W_0(\xi,t)$ and its derivatives may lead to an unsatisfactory discretization form of the regularized Dirac-delta function, especially for a small value of $\alpha$. This is resulted by a non-uniformly distributed grid space used in DQM as follows [51]

$$\xi_i=\frac{1-\cos[(i-1)\pi/(N-1)]}{2},\quad i=1,2,\ldots,N \tag{16}$$

Because most grid points may cluster at the beam ends, errors induced by the grid points become more pronounced when applying a smaller value of $\alpha$ as shown in Figs. 3 and 4. It is therefore not easy to determine an appropriate grid size and the regularized parameter $\alpha$. To overcome this problem, this study proposes the use of the DSC method for the forced vibration analysis of FG beams, which can provide excellent accuracy using the arrangement of equally spaced grid points, i.e., $\xi_i=$

$1/(N-1)$. Figs. 3 and 4 compare the discretized forms of regularized Dirac-delta function by both DQM and DSC with different grid sizes and regularization values ($\alpha$). It is clear that the DSC method shows a good performance. In addition, the discretized errors generated by the DSC method are always in the same order at different locations of the point load.

## 4. Solution Algorithms

### *4.1. Discrete singular convolution*

This section briefly introduces the DSC approach [40, 41]. To approximate an arbitrary function $f(x)$ and its *r*-th order derivatives with respect to a spatial variable at a set of grid points $(\xi_1, \xi_2, \xi_3, \dots, \xi_N)$, a weighted linear combination of the function values at uniformly distributed points $(2M+1)$ is employed, in which $M$ is known as the half computational bandwidth. Then, we have

$$f^{(r)}(x) \approx \sum_{m=-M}^{M} C_m^r f(x_m) \tag{17}$$

where $C_m^r$ denotes the weighting coefficients that can be calculated by the delta kernel of Dirichlet type $\delta_{\alpha,\Delta}^{(r)}(x-x_m)$, and $f(x_m)$ is regarded as a trial function. The *r*-th order derivatives of this DSC kernel with respect to $x$ is given by

$$\delta_{\alpha,\Delta}^{(r)}(x-x_m) = \left(\frac{d}{dx}\right)^r \delta_{\alpha,\Delta}(x-x_m) \tag{18}$$

where $\Delta = 1/(N-1)$ is the grid spacing, $x_m$ is the grid point coordinate and $m = -M, -M+1, \dots, 0, M-1, M$. Therefore, the original function and its *r*-th order derivatives can be approximated by a discretized convolution as follows:

$$f^{(r)}(x) = \sum_{m=-M}^{M} \delta_{\alpha,\Delta}^{(r)}(x-x_m) f(x_m) \tag{19}$$

The DSC formulation is similar to that of DQM. Both approximation frameworks have attracted attentions due to their merits, including high accuracy and simplicity. The DSC approach is regarded as a local-spectral method with a controllable computational bandwidth that possesses good stability and accuracy. The special characteristic of the calculation scheme results in the following banded matrix

$$[\mathbf{C}_{i,m}^{r}] = \begin{bmatrix} C_{1,0}^{r} & C_{1,1}^{r} & \cdots & C_{1,M}^{r} & 0 & \cdots & 0 & \cdots & 0 & \\ C_{2,0}^{r} & C_{2,1}^{r} & \cdots & C_{2,M}^{r} & C_{2,M+1}^{r} & \cdots & 0 & \cdots & 0 & \cdots \\ \vdots & \vdots & \ddots & \vdots & \vdots & \ddots & \ddots & \vdots & \vdots & \\ C_{M,0}^{r} & C_{M,1}^{r} & \cdots & C_{M,M}^{r} & C_{M,M+1}^{r} & \cdots & C_{M,2M}^{r} & 0 & \cdots & \\ 0 & C_{M+1,1}^{r} & \cdots & C_{M+1,M}^{r} & C_{M+1,M+1}^{r} & \cdots & C_{M+1,2M}^{r} & C_{M+1,2M+1}^{r} & 0 & \cdots \\ \vdots & \ddots & \ddots & \vdots & \ddots & \ddots & \vdots & \ddots & \ddots & \\ 0 & 0 & \cdots & 0 & 0 & \cdots & 0 & 0 & \cdots & \\ & \vdots & & \vdots & & \vdots & & \vdots & & \ddots \end{bmatrix} \quad (20)$$

where the total number of grid points does not require to be associated with the matrix band in the DSC method. This enhances the computational efficiency in dealing with large-scale structural calculations. In addition, the use of uniformly distributed points is simple for manipulation.

In the literature, various forms of the DSC kernel have been proposed [50], while the regularized Shannon's delta kernel (RSK) is very efficient because it only generates a small truncation error. The RSK is thus selected as the kernel function in the DSC method for this study as follows

$$\delta_{\alpha,\Delta}(x - x_m) = \frac{\sin\left[\left(\frac{\pi}{\Delta}\right)(x - x_m)\right]}{\left(\frac{\pi}{\Delta}\right)(x - x_m)} \exp\left[-\frac{(x - x_m)^2}{2\sigma^2}\right] \quad (21)$$

where $\sigma$ determines the effective computational bandwidth [52]. For the details of different singular kernels and their applications, we refer readers to Ref. 50. The DSC grid points are taken uniformly spaced in the following form

$$0 = \xi_0 < \xi_1 < \cdots \xi_m < \cdots < \xi_{N-1} = 1, \quad k = 0,1 \ldots, N - 1 \quad (22)$$

Secondly, we define the $N \times N$ differentiation matrices $\mathbf{D}_q^r(q = \xi \ or \ \eta, \ r = 1,2,\dots)$, with their elements given by

$$[\mathbf{D}_q^r] = \delta_{\alpha,\Delta}^{(r)}(q_i - q_m) = \left[\left(\frac{d}{dx}\right)^r \delta_{\alpha,\Delta}(q - q_m)\right]_{q=q_i} = C_m^r \tag{23}$$

For a uniform grid spacing, the matrix is banded to $i - j = m = -M, \dots, 0, \dots M$. As presented in Eq. (19), there exist $M$ fictitious points out of the physical domain when applying the DSC method. A complete scheme for the elimination of ghost points can be found in the literature [52-54]. For the treatment of simply supported and clamped edges, the method of symmetric and anti-symmetric extensions can be well applied, respectively. Taking the left side of the beam as an example, the relationship between inner points and fictitious points is assumed as

$$W(\xi_{-m}) - W(\xi_0) = a_m[W(\xi_m) - W(\xi_0)] \tag{24}$$

which can be rewritten as,

$$W(\xi_{-m}) = a_m W(\xi_m) + (1 - a_m) W(\xi_0) \tag{25}$$

In terms of the DSC approach, the first- and second-order derivatives of $W$ can be approximated as

$$\begin{aligned} W'(\xi) &= \sum_{m=-M}^{M} C_m^1 W(\xi_m) \\ &= \left[C_0^1 - \sum_{m=1}^{M}(1 - a_m)C_m^1\right] W(\xi_0) + \sum_{m=1}^{M}(1 - a_m)C_m^1 W(\xi_m) \end{aligned} \tag{26}$$

$$\begin{aligned} W''(\xi) &= \sum_{m=-M}^{M} C_m^2 W(\xi_m) \\ &= \left[C_0^2 + \sum_{m=1}^{M}(1 - a_m)C_m^2\right] W(\xi_0) + \sum_{m=1}^{M}(1 - a_m)C_m^2 W(\xi_m) \end{aligned} \tag{27}$$

Consider an elastically supported FG beam with rotational stiffness $K(s)$. The boundary conditions in a dimensionless form are

$$W(\xi) = 0,\ \ EI\frac{d^2W(\xi)}{d\xi^2} - K(s)L\frac{dW(\xi)}{d\xi} = 0\ \ (at\ \xi = 0\ and\ \xi = 1) \tag{28}$$

Substitution of Eqs. (26) – (27) into Eq. (28) and after simplification, we obtain the following expression

$$a_m = \frac{K'C_m^1 - C_m^2}{K'C_m^1 + C_m^2} \quad (m = 1,2, \dots, M) \tag{29}$$

where $K' = K(s)/EI$ is the non-dimensionalized rotational restraint stiffness parameter, and $C_m^n(n = 1, 2)$ are defined in Eq. (23). In a similar manner, it is easy to obtain $a_m = 1$ for a clamped condition and $a_m = -1$ for a simple support. We also summarize various cases of supporting boundaries in Table 1 for reference. The implementation of boundary conditions for a free-edged beam can be treated by the Taylor series expansion method [44, 45, 55]. As many real scenarios of moving load problems are simply supported or fixed cases, so the free boundary condition is not considered in this work.

The governing equilibrium Eq. (15) presented in a matrix notation is given by

$$[\mathbf{K}]\{\boldsymbol{W}_\mathbf{0}(t)\} + [\mathbf{M}]\{\ddot{\boldsymbol{W}}_\mathbf{0}(t)\} = \{\boldsymbol{F}(t)\} \tag{30}$$

where $[\mathbf{K}]$ and $[\mathbf{M}]$ are, respectively, the stiffness and mass matrices of the FG beam as follows

$$[\mathbf{K}] = \left(D_{11} - \frac{B_{11}^2}{A_{11}}\right)[\mathbf{D}_\xi^4], \quad [\mathbf{M}] = I_0L^4[\mathbf{I}] \tag{31}$$

in which $[\mathbf{I}]$ represents an $n \times n$ identity matrix, and $\{\boldsymbol{W}_\mathbf{0}(t)\}$ and $\{\ddot{\boldsymbol{W}}_\mathbf{0}(t)\}$ in Eq. (30) are, respectively, the transverse deflection and acceleration vectors as

$$\{\boldsymbol{W_0}(t)\} = \{W_0(\xi_0, t) \quad W_0(\xi_2, t) \quad \cdots \quad W_0(\xi_{N-1}, t)\}^T \tag{32}$$

$$\{\ddot{\boldsymbol{W}}_{\boldsymbol{0}}(t)\} = \{\ddot{W}_0(\xi_0, t) \quad \ddot{W}_0(\xi_2, t) \quad \cdots \quad \ddot{W}_0(\xi_{N-1}, t)\}^T \tag{33}$$

In Eq. (30), $\{\boldsymbol{F}(t)\}$ denotes the load vector that is approximated by the regularized Gauss' delta function via Eq. (13) as

$$\{\boldsymbol{F}(t)\} = -\frac{fL^3}{\sqrt{2\pi}\varepsilon}\left\{\exp\left[-\frac{\left(\xi_0 - \xi_p(t)\right)^2}{2\varepsilon^2}\right] \quad \cdots \quad \exp\left[-\frac{\left(\xi_{N-1} - \xi_p(t)\right)^2}{2\varepsilon^2}\right]\right\}^T \tag{34}$$

Mathematically, Eq. (30) is a second-order differential equation with the time-dependent coefficient matrices, which can be solved by using various step-by-step time integration schemes. The present study employs the Newmark-$\beta$ integration scheme for this problem.

For free vibration analysis, the magnitude of the external force $f$ is assumed to be zero and the time-dependent displacement can be expressed as follows

$$W_0(\xi, t) = W(\xi)\cos\omega t \tag{35}$$

where $\omega$ is the natural frequency of the beam. With the aid of Eq. (35), the governing equation (Eq. (15)) can be rewritten as

$$\frac{\partial^4 W(\xi)}{\partial \xi^4} = \frac{I_0}{GA\rho_b}\lambda^2 W(\xi) \tag{36}$$

where $\lambda = \omega L^2\sqrt{\rho_b A/E_b I}$ represents the dimensionless frequency parameter, $G = 12(D_{11} - B_{11}^2/A_{11})/E_b h^3 b$ is a non-uniform distribution factor of FG materials. Obviously, the value of $G$ is equal to 1 in the case of homogenous properties across the beam section. In terms of a matrix form, Eq. (36) can be expressed as follows

$$[\tilde{\mathbf{K}}]\{\boldsymbol{W_0}\} = \Omega^2\{\boldsymbol{W_0}\} \tag{37}$$

where $[\tilde{\mathbf{K}}]$ is a stiffness matrix and $\Omega$ is a non-dimensional natural frequency in the following form

$$\left[\widetilde{\mathbf{K}}\right] = \left[\mathbf{D}_{\xi}^{4}\right], \quad \Omega = \lambda\sqrt{I_0/G\rho_b A} \tag{38}$$

The solutions of Eq. (37) can be obtained by a standard eigenvalue solver.

*4.2.Implicit time integration – Newmark-$\beta$ method*

The Newmark-$\beta$ integration scheme [48] is used to solve the equations motion in this study and is briefly introduced in this section. This approach as one of the popular numerical techniques can perform the time discretization of motion equations with good accuracy for linear problems. The standard form of the finite difference approximations for the Newmark-$\beta$ method can be derived in terms of displacement and velocity at $t + \Delta t$ as

$$\boldsymbol{W}_{t+\Delta t} = \boldsymbol{W}_t + \Delta t\dot{\boldsymbol{W}}_{\boldsymbol{t}} + \Delta t^2\left[\left(\frac{1}{2} - \beta\right)\ddot{\boldsymbol{W}}_t + \beta\ddot{\boldsymbol{W}}_{t+\Delta t}\right] \tag{39}$$

$$\dot{\boldsymbol{W}}_{t+\Delta t} = \dot{\boldsymbol{W}}_t + \Delta t\left[(1-\gamma)\ddot{\boldsymbol{W}}_t + \boldsymbol{\gamma}\ddot{\boldsymbol{W}}_{t+\Delta t}\right] \tag{40}$$

where $\beta$ and $\gamma$ are two controllable parameters. For $\beta = 1/4$ and $\gamma = 1/2$, this is an average acceleration scheme that is unconditionally stable and second-order accurate [56]. Based on this numerical framework, the governing Eq. (30) can be further written as

$$[\overline{\mathbf{K}}]\{\boldsymbol{W}_{t+\Delta t}\} = \{\overline{\boldsymbol{F}}_{t+\Delta t}\} \tag{41}$$

where $[\overline{\mathbf{K}}]$ and $\{\overline{\boldsymbol{F}}_{t+\Delta t}\}$ are, respectively, the updated stiffness matrix and effective load vector as follows

$$[\overline{\mathbf{K}}] = \alpha_1[\mathbf{M}] + \alpha_4[\mathbf{C}] + [\mathbf{K}] \tag{42}$$

$$\begin{aligned}\{\overline{\boldsymbol{F}}_{t+\Delta t}\} = [\mathbf{M}]\left(\alpha_1\{\boldsymbol{W}_t\} + \alpha_2\{\dot{\boldsymbol{W}}_t\} + \alpha_3\{\ddot{\boldsymbol{W}}_t\}\right) + [\mathbf{C}](\alpha_4\{\boldsymbol{W}_t\} + \alpha_5\{\dot{\boldsymbol{W}}_t\} \\ + \alpha_6\{\ddot{\boldsymbol{W}}_t\}\end{aligned} \tag{43}$$

where $[\mathbf{C}]$ is a damping matrix of the dynamic system, which is assumed as an $n \times n$ zero matrix in the present study. In Eqs. (42) and (43), the coefficients $\alpha_1$, $\alpha_2, \ldots \alpha_6$ are given by

$$\alpha_1 = \frac{1}{\beta \Delta t^2}, \alpha_2 = \frac{1}{\beta \Delta t}, \alpha_3 = \frac{1}{2\beta} - 1, \alpha_4 = \frac{\gamma}{\beta \Delta t^2}, \alpha_5 = \frac{\gamma}{\beta} - 1, \alpha_6 = \frac{\gamma}{2\beta} - 1 \quad (44)$$

## 5. Numerical Results and Discussion

For verification, some numerical examples by the DSC approach discussed above are selected for analysis in this section. The first one is the free vibration analysis of simply supported beams to validate the accuracy and convergence. The influence of material distribution on the vibration frequency of FG beams is thus investigated. Secondly, the moving load problem of a homogenous beam is analyzed. The calculated mid-span deflections are compared with those of analytical or numerical ones. At the same time, the optimization of the regularized parameter $\alpha$ in an approximation of the moving load vectors by the regularized Dirac-delta function is discussed. The last examples consider different material distribution for the vibration analysis of FG beams due to a moving load, in which the results of FG beams with a simply supported boundary are compared with those from the open literature. Some first accurate known results for elastically restrained FG beams are also presented.

### *5.1. Free vibration analysis of homogenous and FG beams*

Before applying the proposed DSC method, a convergence study is conducted to find the optimal values of $M$ and $N$. Fig. 5 shows the convergence study of non-dimensional natural frequencies for a simply supported beam by altering $M$ from 1 to 32. It is observed that the results converge when the half bandwidth $M \geq 16$. To verify the accuracy of solutions, Table 2 summarizes the numerical results for $N = 99$ and $M \in [12, 32]$. As compared with the results from the published article [59], it can be found that the DSC method is able to yield accurate and reliable results. Fig. 6 shows the effect of grid size $N$ when the bandwidth is set as $M$=20. It is clear that the grid size $N$ has little influence on the first five natural frequency parameters. Based on these results, the values of $M = 32$ and $N = 51$ are thus selected for subsequent analysis in this study.

For FG beams, the properties are assumed to vary through the thickness. The top surface of FG beams is pure alumina ($\mathrm{Al_2O_3}$) with the material properties $E_t = 380\ \mathrm{GPa}$ and $\rho_t = 3960\ \mathrm{kg/m^3}$, while the bottom surface of FG beams is made of 100% Aluminum ( Al ) with the material parameters $E_b = 70\ \mathrm{GPa}$ and $\rho_b = 2702\ \mathrm{kg/m^3}$. The Poisson's ratio ($\nu$) of FG beams is supposed to be constant ($= 0.3$). Fig. 2 illustrates the influence of parameters on the variation of material properties of the FG beams, including elasticity modulus and mass density. Table 3 presents the non-dimensional natural frequencies of simply supported FG beams for different values of the power-law index $k$. A comparative analysis of the calculated results is conducted with those of Simsek [57] and Thai and Vo [58], in which the beam model is based on the classical beam theory with a span-to-depth ratio $L/h = 20$. On the other hand, the non-dimensional vibration frequencies of clamped FG beams are provided in Table 4. A good consistence between the DSC results and the available solutions is observed. Some first-known results are also provided. This study further predicts the vibration frequencies of FG beams restrained by elastic ends as shown in Table 5. The fundamental non-dimensional frequencies of FG beams for the rotational restraint stiffness parameters $K' \in [0, 10^5]$, and the different distribution patterns of material properties obtained by the power and exponential laws are presented. The results reveal that the fundamental frequency will increase as $K'$ increases. When the value of $K'$ approaches to 0 and infinity, the fundamental frequencies of the FG beam are close to those acquired from the simply supported and clamped cases respectively. This is easily explained by Eq. (29). In Tables 3 – 5, it is also observed that increasing the power-law index leads to a decrease of the natural frequencies of FG beams. It is known that the higher value of power-law index results in an increase of bending rigidity, which is consistent with the results in Fig. 2.

*5.2. Vibration analysis of homogeneous beams due to a moving load*

In this section, some examples are presented to demonstrate the reliability and flexibility of the proposed method for the forced vibration analysis of beams due to a moving point load. This study uses the regularized Dirac-delta function to approximate the moving load effect, and the influence of the regularization parameter $\alpha$ on the calculation accuracy needs to be investigated.

We consider a simply supported beam with a span length $L = 101.6\text{mm}$, a square cross-section with width and thickness as $b = h = 6.35$ mm, the mass density $\rho = 10686.9\ \text{kg/m}^3$, the elasticity modulus $E = 2.068 \times 10^{11}$ Pa, and it is subjected to a concentrated point load $f = 4.45\,\mathrm{N}$ with a moving velocity $v_p$ for validation purpose [37]. The approximated form of the dynamic equation of the beam system in terms of the DSC method is eventually solved by the Newmark-$\beta$ integration scheme with a time step of $n_t = 500$. The present results are compared with those numerical and exact solutions.

Fig. 7 shows the dynamic responses at the central point of a simply supported beam under a moving load with various velocities. The displacement ($w_{cd}$) is normalized by the static deflection (i.e., $w_{cs} = fL^3/(48EI)$) resulted by a point load $f$ at the mid-span of the beam. Note that the numerical results for each case are obtained using different values (0.012 to 0.2) of the regularized parameter ($\alpha$) to investigate the accuracy and convergence. It is observed that the mid-span displacements will converge for a relatively small value of $\alpha$. This is consistent with the conclusion that a small value of $\alpha$ can provide a better representation of the original continuous model (i.e., Dirac-delta function). Table 6 summarizes the results generated by the proposed method and a rapid convergence of the solutions with respect to the regularized parameter ($\alpha$) can be observed as compared to Refs. 5 and 37. Accordingly, the computational results of clamped beams are presented in Table 7, where the deflection ($w_{cd}$) is also normalized by the static deflection (i.e., $w_{cs} = fL^3/(192EI)$. Since there is no analytical solution for the moving load problem of clamped beams, numerical results are used for validation [8]. It is found that the faster the moving velocity is, the larger mid-span displacement will be achieved. It is worth noting that the uniformly distributed grid points ($N$) employed in the DSC method allow a smaller value of the regularized parameter ($\alpha$) to achieve a higher level of accuracy. Therefore, it is concluded that the DSC regularized Dirac-delta method is a promising technique for solving moving load problems. According to the results in this section, $\alpha = 0.012$ is selected for further analysis.

*5.3. Vibration analysis of FG beams under a moving force*

This section further extends to investigate the dynamic characteristics of FG beams subjected to a moving load. The influence of different parameters (material properties and moving load velocity) on the dynamic behavior of FG beams is investigated. In the work of Simsek and Kocatürk [24], the relationship between the moving load velocity and the maximum normalized dynamic displacement at the mid-span of FG beams under various power-law indices was found. For convenience, the material properties and dimensions of FG beams are the same as those presented in Ref. 24. The top surface of FG beams is made of pure alumina ($\mathrm{Al_2O_3}$) with the material properties $E_t = 390\ \mathrm{GPa}$ and $\rho_t = 3960\ \mathrm{kg/m^3}$, and the bottom surface of FG beams is 100% Aluminum (Al) with the material parameters $E_b = 210\ \mathrm{GPa}$ and $\rho_b = 7800\ \mathrm{kg/m^3}$. The Poisson's ratio ($\nu$) of FG beams is $0.3$. The dimensions are length $L = 20\mathrm{m}$, width $b = 0.4\mathrm{m}$ and height $h = 0.9\mathrm{m}$. The magnitude of the moving force is $f = 10^5\mathrm{N}$.

Tables 9 – 15 summarize the deflections at the mid-span of FG beams for various moving load velocities, power-law indices and boundary conditions, where the mid-point displacements are normalized by the static ones as shown in Table 1. Note that the material properties of FG beams are full alumina when $k$ tends to zero, while it becomes a full metal beam when $k$ goes to infinity. Increasing the power-law index leads to a larger deflection of the FG beam at the center position with the same moving velocity. The maximum magnitudes of normalized mid-span deflection of simply supported FG beams excited by a moving load with critical velocity are underlined in Table 9. For verification purpose, we extracted the data and summarized them in Table 8 to compare with the published results. Table 10 further confirms the accuracy and reliability of the DSC method by considering the moving load problem of simply supported FG beams. It is clear that good agreement is achieved between the DSC-based results and the solutions given in Refs. 24 and 28.

Fig. 8 demonstrates the dynamic performance of simply supported FG beams excited by a moving load with various speeds. It is observed that the variation of the power-law parameter greatly affects the dynamic behavior of FG beams by changing their material properties. When the power-law parameter $k$ increases, the maximum normalized dynamic deflection at the center of FG beams will increase. It is noted that a faster moving load will take less travelling time, the local fluctuation of FG beams is not as obvious as that of the slower case (cf. Fig. 8(a) with a speed of 16.3 m/s and Fig. 8(d) with a speed of 84.8 m/s). Similar patterns are observed in Figs. 9 and 10 for the deflection of elastically restrained FG beams. The maximum deflection of FG beams excited by a moving load under the critical velocity, e.g., the values presented in Tables 8 – 9, can be controlled by selecting an appropriate value of the power-law parameter $k$. Note that Table 11 provides new results for clamped FG beams under a moving load since there are no numerical or analytical results available. To further investigate the dynamic response of FG beams with elastically restrained supports, some numerical examples applying various speeds of moving loads are demonstrated herein. The material properties of the beam are assumed to be the same as those employed in simply supported and clamped beams. In Tables 12 – 15, it is found that increasing the running speed of the moving load can result in a larger displacement of the elastically restrained FG beam at the center position. When the rotational restraint stiffness parameter $K'$ goes to infinite, the normalized mid-span deflection of elastically restrained FG beams is very close to the results obtained from the clamped case, see Tables 11 and 15. These first-known results may serve as benchmark solutions for future reference.

## 6. Conclusions

This paper shows the effectiveness and feasibility of the DSC method with a regularized Dirac-delta function for the dynamic analysis of elastically restrained FG beams under a moving load. The regularization of the Dirac-delta function regarded as a Dirichlet type is employed as a delta kernel function to formulate the DSC algorithm. From a computational point of view, a simple distribution scheme of grid points based on the DSC method can provide a good representation of moving load vectors when using the regularized Dirac-delta function. The DSC method is simple and stable for solving complex geometries and boundary conditions. Moreover, the special characteristics in the DSC approximation scheme can generate a sparse matrix that enables trade-offs between computational effort and accuracy.

In this work, the resulting time-dependent dynamic equations are solved by the Newmark-$\beta$ integration scheme. The elastically restrained condition as well as other two types of boundary conditions (simply supported and clamped edges) are imposed. In addition, a parametric analysis for moving load velocity, material properties and spring stiffness on the dynamic behavior of FG beams is extensively investigated. We found that the maximum deflection of FG beams excited by a moving load under a critical velocity scenario can be controlled by the power-law parameter ($k$). The DSC-based results agree well with those presented in the literature, and some new accurate results are provided as well.

Future studies will extend to the vibration and buckling analysis of cracked FG beams under a moving load. A higher-order beam theory will be employed to conduct a comprehensive analysis. In real-engineering environments, cracks or defects are likely to be present on surfaces or internal levels of structural components. For example, beam-like structures such as the track/rail system suffered from wheel-rail interactions are expected to develop progressive cracks due to fatigue or stress concentration under in-service loading conditions. The occurence of cracks will change the local structural stiffness that can significantly affect the stability and integrity of structures. Hence, understanding of the dynamic characteristics of cracked beam-type structures under a moving load is necessary.

**Acknowledgements**

The work described in this paper was supported by the Research Impact Fund (Project No. R-5020-18) from the Research Grants Council of the Hong Kong Special Administrative Region. The funding support from the Innovation and Technology Commission of the HKSAR Government to the Hong Kong Branch of National Rail Transit Electrification and Automation Engineering Technology Research Center (Grant Nos. K-BBY1 and 1-BBVQ) is also gratefully acknowledged.

## References

[1] Madrazo-Aguirre F, Ruiz-Teran AM, Wadee MA. Dynamic behaviour of steel–concrete composite under-deck cable-stayed bridges under the action of moving loads. Engineering Structures. 2015;103:260-74.

[2] Konstantakopoulos T, Raftoyiannis I, Michaltsos G. Suspended bridges subjected to earthquake and moving loads. Engineering Structures. 2012;45:223-37.

[3] Yau J, Martínez-Rodrigo MD, Doménech A. An equivalent additional damping approach to assess vehicle-bridge interaction for train-induced vibration of short-span railway bridges. Engineering Structures. 2019;188:469-79.

[4] Yang D-S, Wang CJES. Dynamic response and stability of an inclined Euler beam under a moving vertical concentrated load. 2019;186:243-54.

[5] Frýba L. Vibration of Solids and Structures Under Moving Loads: Thomas Telford; 1999.

[6] Meirovitch L. Analytical methods in vibrations. 1967.

[7] Pala Y, Reis M. Dynamic response of a cracked beam under a moving mass load. Journal of Engineering Mechanics. 2012;139:1229-38.

[8] Rieker JR, Lin Y-H, Trethewey MW. Discretization considerations in moving load finite element beam models. Finite elements in analysis design. 1996;21:129-44.

[9] Kocatürk T, Şimşek M. Dynamic analysis of eccentrically prestressed viscoelastic Timoshenko beams under a moving harmonic load. Computers and Structures. 2006;84:2113-27.

[10] Yang J, Chen Y, Xiang Y, Jia X. Free and forced vibration of cracked inhomogeneous beams under an axial force and a moving load. Journal of Sound Vibration. 2008;312:166-81.

[11] Kim S-M. Stability and dynamic response of Rayleigh beam–columns on an elastic foundation under moving loads of constant amplitude and harmonic variation. Engineering Structures. 2005;27:869-80.

[12] Kim S-M. Vibration and stability of axial loaded beams on elastic foundation under moving harmonic loads. Engineering Structures. 2004;26:95-105.

[13] Corrêa RT, Simões F, da Costa AP. Moving loads on beams on Winkler foundations with passive frictional damping devices. Engineering Structures. 2017;152:211-25.

[14] Aied H, González A. Theoretical response of a simply supported beam with a strain rate dependant modulus to a moving load. Engineering Structures. 2014;77:95-108.

[15] Svedholm C, Zangeneh A, Pacoste C, François S, Karoumi R. Vibration of damped uniform beams with general end conditions under moving loads. Engineering Structures. 2016;126:40-52.

[16] Yang D-S, Wang C. Dynamic response and stability of an inclined Euler beam under a moving vertical concentrated load. Engineering Structures. 2019;186:243-54.

[17] Ouyang H. Moving-load dynamic problems: a tutorial (with a brief overview). Mechanical Systems and Signal Processing. 2011;25:2039-60.

[18] Koizumi M. FGM activities in Japan. Composites Part B: Engineering. 1997;28:1-4.

[19] Koizumu M. The concept of FGM, ceramic transactions. Funct Grad Mater. 1993;34:3-10.

[20] Wang C, Ke L, Chowdhury AR, Yang J, Kitipornchai S, Fernando D. Critical examination of midplane and neutral plane formulations for vibration analysis of FGM beams. Engineering Structures. 2017;130:275-81.

[21] Ke L-L, Yang J, Kitipornchai S. Nonlinear free vibration of functionally graded carbon nanotube-reinforced composite beams. Composite Structures. 2010;92:676-83.

[22] Mao J-J, Ke L-L, Yang J, Kitipornchai S, Wang Y-S. Thermoelastic instability of functionally graded materials with interaction of frictional heat and contact resistance. Mechanics Based Design of Structures Machines. 2018;46:139-56.

[23] Wu H, Kitipornchai S, Yang J. Free vibration and buckling analysis of sandwich beams with functionally graded carbon nanotube-reinforced composite face sheets. International Journal of Structural Stability Dynamics. 2015;15:1540011.

[24] Simsek M, Kocatürk T. Free and forced vibration of a functionally graded beam subjected to a concentrated moving harmonic load. Composite Structures. 2009;90:465-73.

[25] Şimşek M. Non-linear vibration analysis of a functionally graded Timoshenko beam under action of a moving harmonic load. Composite Structures. 2010;92:2532-46.

[26] Şimşek M, Aydın M. Size-dependent forced vibration of an imperfect functionally graded (FG) microplate with porosities subjected to a moving load using the modified couple stress theory. Composite Structures. 2017;160:408-21.

[27] Şimşek M, Kocatürk T, Akbaş Ş. Dynamic behavior of an axially functionally graded beam under action of a moving harmonic load. Composite Structures. 2012;94:2358-64.

[28] Khalili S, Jafari A, Eftekhari S. A mixed Ritz-DQ method for forced vibration of functionally graded beams carrying moving loads. Composite Structures. 2010;92:2497-511.

[29] Wang Y, Wu D. Thermal effect on the dynamic response of axially functionally graded beam subjected to a moving harmonic load. Acta Astronautica. 2016;127:171-81.

[30] Nguyen DK, Nguyen QH, Tran TT, Bui VT. Vibration of bi-dimensional functionally graded Timoshenko beams excited by a moving load. Acta Mechanica. 2017;228:141-55.

[31] Songsuwan W, Pimsarn M, Wattanasakulpong N. Dynamic Responses of Functionally Graded Sandwich Beams Resting on Elastic Foundation Under Harmonic Moving Loads. International Journal of Structural Stability and Dynamics. 2018;18:1850112.

[32] Yang Y, KouPang K, Lam C, Iu V. Dynamic behaviors of tapered bi-directional functionally graded beams with various boundary conditions under action of a moving harmonic load. Engineering Analysis with Boundary Elements. 2019;104:225-39.

[33] Jafari A, Eftekhari S. A new mixed finite element–differential quadrature formulation for forced vibration of beams carrying moving loads. Journal of Applied Mechanics. 2011;78:011020.

[34] Wang X, Jin C. Differential quadrature analysis of moving load problems. Advances in Applied Mathematics and Mechanics. 2016;8:536-55.

[35] Wang X, Liang X, Jin C. Accurate dynamic analysis of functionally graded beams under a moving point load. Mechanics Based Design of Structures Machines. 2017;45:76-91.

[36] Song Y, Kim T, Lee U. Vibration of a beam subjected to a moving force: frequency-domain spectral element modeling and analysis. International Journal of Mechanical Sciences. 2016;113:162-74.

[37] Eftekhari S. A differential quadrature procedure with regularization of the Dirac-delta function for numerical solution of moving load problem. Latin American Journal of Solids and Structures. 2015;12:1241-65.

[38] Wei G, Zhao Y, Xiang Y. A novel approach for the analysis of high-frequency vibrations. Journal of Sound Vibration. 2002;257:207-46.

[39] Wang X. Novel discrete singular convolution for high-frequency vibration analysis of structural elements. AIAA Journal. 2017:4364-75.

[40] Wei G. Discrete singular convolution for the solution of the Fokker–Planck equation. The Journal of chemical physics. 1999;110:8930-42.

[41] Wei G. A unified approach for the solution of the Fokker-Planck equation. Journal of Physics A: Mathematical General. 2000;33:4935.

[42] Ng C, Zhao Y, Wei G. Comparison of discrete singular convolution and generalized differential quadrature for the vibration analysis of rectangular plates. Computer Methods in Applied Mechanics Engineering. 2004;193:2483-506.

[43] Lai SK, Xiang Y. DSC analysis for buckling and vibration of rectangular plates with elastically restrained edges and linearly varying in-plane loading. International Journal of Structural Stability Dynamics. 2009;9:511-31.

[44] Wang X, Xu S. Free vibration analysis of beams and rectangular plates with free edges by the discrete singular convolution. Journal of Sound ibrational. 2010;329:1780-92.

[45] Wang X, Yuan Z. Discrete singular convolution and Taylor series expansion method for free vibration analysis of beams and rectangular plates with free boundaries. International Journal of Mechanical Sciences. 2017;122:184-91.

[46] Gao K, Li R, Yang J. Dynamic characteristics of functionally graded porous beams with interval material properties. Engineering Structures. 2019;197:109441.

[47] Kara M, Seçgin A. Discrete singular convolution method for one-dimensional vibration and acoustics problems with impedance boundaries. Journal of Sound Vibration. 2019;446:22-36.

[48] Newmark NM. A method of computation for structural dynamics. American Society of Civil Engineers; 1959.

[49] Reddy JN. Energy principles and variational methods in applied mechanics: John Wiley & Sons; 2017.

[50] Wei G, Zhao Y, Xiang Y. Discrete singular convolution and its application to the analysis of plates with internal supports. Part 1: Theory and algorithm. International Journal for Numerical Methods in Engineering. 2002;55:913-46.

[51] Bert CW, Malik M. Differential quadrature method in computational mechanics: a review. Applied mechanics reviews. 1996;49:1-28.

[52] Wei G, Zhao Y, Xiang Y. The determination of natural frequencies of rectangular plates with mixed boundary conditions by discrete singular convolution. International Journal of Mechanical Sciences. 2001;43:1731-46.

[53] Xiang Y, Zhao Y, Wei G. Discrete singular convolution and its application to the analysis of plates with internal supports. Part 2: Applications. International Journal for Numerical Methods in Engineering. 2002;55:947-71.

[54] Zhao Y, Wei G. DSC analysis of rectangular plates with non-uniform boundary conditions. Journal of Sound Vibration. 2002;255:203-28.

[55] Lai SK, Zhang LH. Thermal effect on vibration and buckling analysis of thin isotropic/orthotropic rectangular plates with crack defects. Engineering Structures. 2018;177:444-58.

[56] Gavin H. Numerical integration for structural dynamics. Department of Civil Environmental Engineering, Duke University: Durham, NC, USA. 2001.

[57] Simsek M. Fundamental frequency analysis of functionally graded beams by using different higher-order beam theories. Nuclear Engineering Design. 2010;240:697-705.

[58] Thai H-T, Vo TP. Bending and free vibration of functionally graded beams using various higher-order shear deformation beam theories. International Journal of Mechanical Sciences. 2012;62:57-66.

[59] Leissa AW. The free vibration of rectangular plates. Journal of sound vibration. 1973;31:257-93.

**Captions of Figures**

**Fig. 1.** Schematic of a functionally graded beam under a concentrated moving load.

**Fig. 2.** Variation of material properties of FG beams: a) Elasticity Modulus; b) Mass Density.

**Fig. 3.** Comparison of the loading approximation using the regularized Dirac-delta function ($\alpha = 0.25$) by DQM and DSC: a) – b) point load at $x_p/L = 0.5$; c) – d) point load at $x_p/L = 0.25$.

**Fig. 4.** Comparison of the loading approximation using the regularized Dirac-delta function ($\alpha = 0.05$) by DQM and DSC: a) – b) point load at $x_p/L = 0.5$; c) – d) point load at $x_p/L = 0.25$.

**Fig. 5.** Convergence study of first five non-dimensional frequencies for a simply supported beam ($N = 99$).

**Fig. 6.** Convergence study of non-dimensional frequency parameters for a simply supported beam ($M = 20$).

**Fig. 7.** Convergence study of the regularized parameter ($\alpha$) for the normalized central beam deflection of a simply supported beam under a moving load by DSC method ($M = 32, N = 51$): a) $v_p = 15.6\mathrm{m/s}$, b) $v_p = 31.2\mathrm{m/s}$, c) $v_p = 46.8\mathrm{m/s}$ and d) $v_p = 62.4\mathrm{m/s}$.

**Fig. 8.** Normalized mid-span deflection of a simply supported FG beam with various material properties under a travelling load: a) $v_p = 16.3\mathrm{m/s}$, b) $v_p = 42.4\mathrm{m/s}$, c) $v_p = 65.8\mathrm{m/s}$ and d) $v_p = 84.8\mathrm{m/s}$.

**Fig. 9.** Normalized mid-span deflection of elastically restrained FG beams ($K'$=10) with various material properties under a travelling load: a) $\mathrm{v_p} = 108.6\mathrm{m/s}$, b) $\mathrm{v_p} = 130.3\mathrm{m/s}$, c) $\mathrm{v_p} = 156.4\mathrm{m/s}$ and d) $\mathrm{v_p} = 187.7\mathrm{m/s}$.

**Fig. 10.** Normalized mid-span deflection of elastically restrained FG beams ($K'$=$10^3$) with various material properties under a travelling load: a) $\mathrm{v_p} = 108.6\mathrm{m/s}$, b) $\mathrm{v_p} = 130.3\mathrm{m/s}$, c) $\mathrm{v_p} = 156.4\mathrm{m/s}$ and d) $\mathrm{v_p} = 187.7\mathrm{m/s}$.

**Captions of Tables**

**Table 1** Inter-relationship coefficients ($a_m$) and static deflections ($w_{cs}$) under various boundary conditions.

**Table 2** Convergence and comparison of frequency parameters $\Omega$ for a simply supported homogeneous beam with $N = 99$.

**Table 3** First five non-dimensional natural frequencies of simply supported FG beams.

**Table 4** First five non-dimensional natural frequencies of clamped FG beams.

**Table 5** Fundamental non-dimensional frequencies of elastically restrained FG beams.

**Table 6** Convergence and comparison for the maximum value of the normalized mid-span displacement of a simply supported beam under a moving load ($M = 32, N = 51$).

**Table 7** Convergence and comparison for the maximum value of the normalized mid-span displacement of a clamped beam under a moving load ($M = 32, N = 51$).

**Table 8** Maximum normalized mid-span deflection of simply supported FG beams with different material properties and moving loads.

**Table 9** Maximum normalized mid-span deflection of simply supported FG beams excited by moving load with critical velocities.

**Table 10** Maximum normalized mid-span deflection of simply supported FG beams.

**Table 11** Maximum normalized mid-span deflection of clamped FG beams.

**Table 12** Maximum normalized mid-span deflection of elastically restrained FG beams ($K' = 10$).

**Table 13** Maximum normalized mid-span deflection of elastically restrained FG beams ($K' = 10^2$).

**Table 14** Maximum normalized mid-span deflection of elastically restrained FG beams ($K' = 10^3$).

**Table 15** Maximum normalized mid-span deflection of elastically restrained FG beams ($K' = 10^4$).

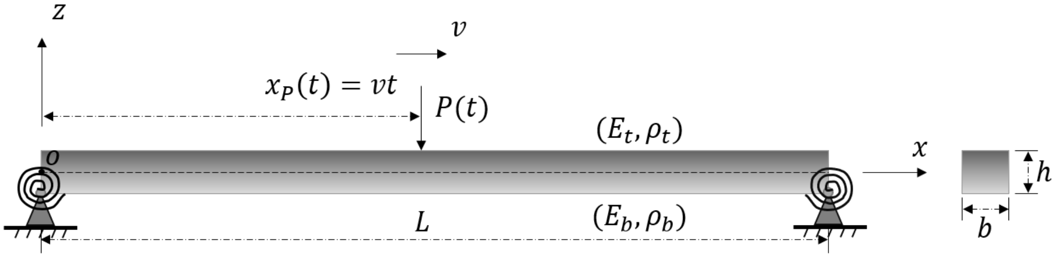


**Fig. 1.** Schematic of a functionally graded beam with elastic restraints under a concentrated moving load.

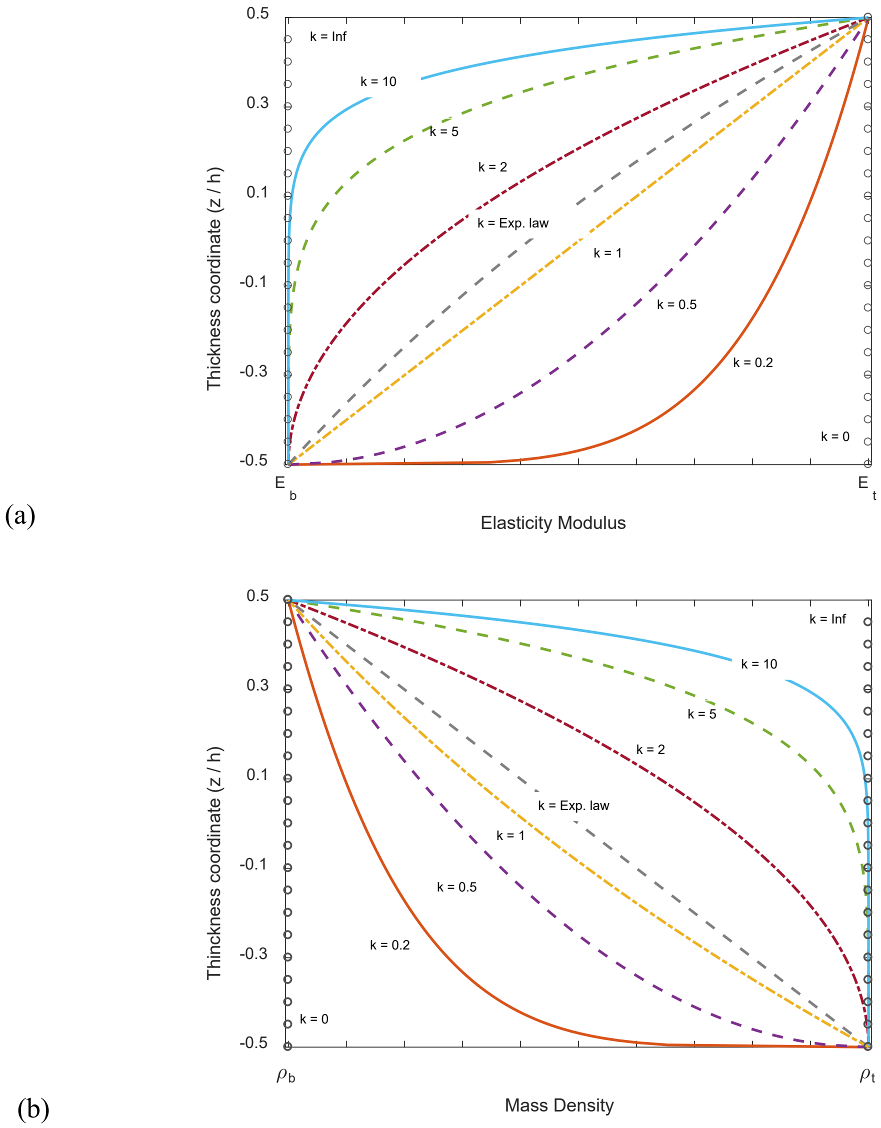


**Fig. 2.** Variation of material properties of FG beams: a) Elasticity Modulus; b) Mass Density.

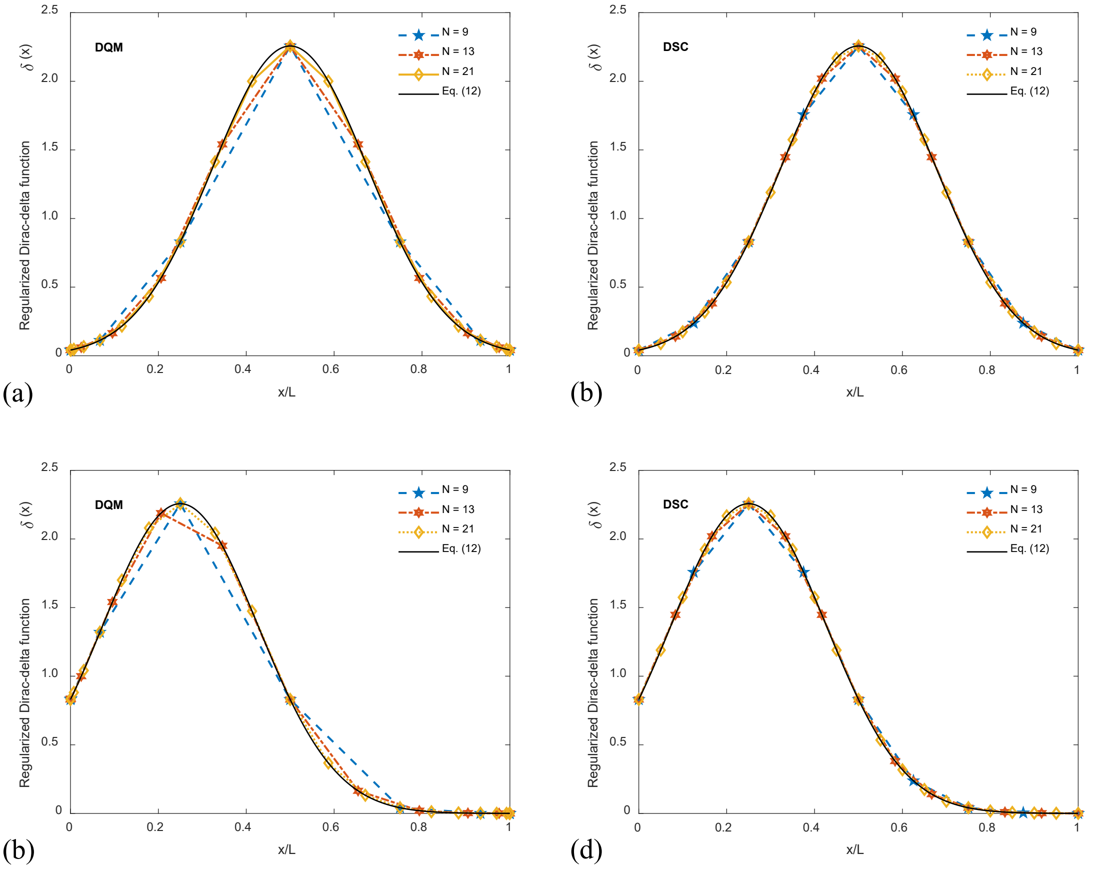


**Fig. 3.** Comparison of the loading approximation using the regularized Dirac-delta function ($\alpha = 0.25$) by DQM and DSC: a) – b) point load at $x_p/L = 0.5$; c) – d) point load at $x_p/L = 0.25$.

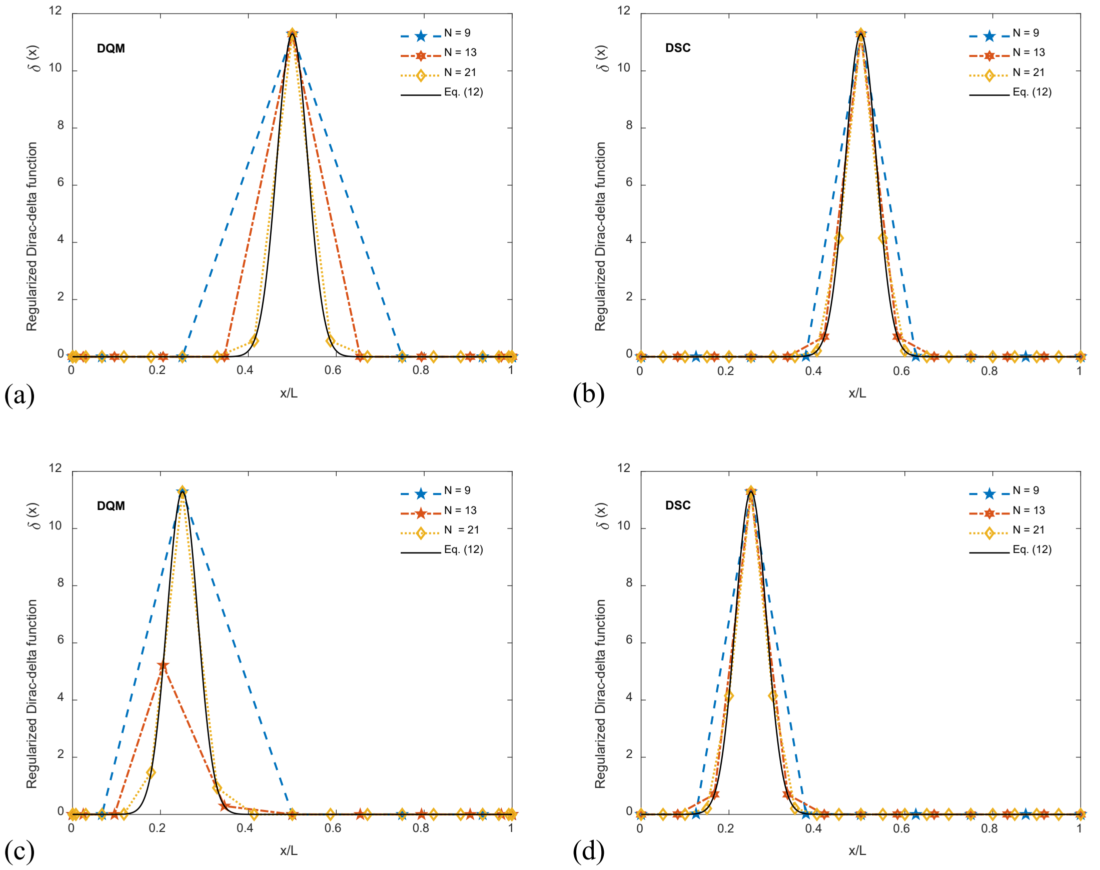


**Fig. 4.** Comparison of the loading approximation using the regularized Dirac-delta function ($\alpha = 0.05$) by DQM and DSC: a) – b) point load at $x_p/L = 0.5$; c) – d) point load at $x_p/L = 0.25$.

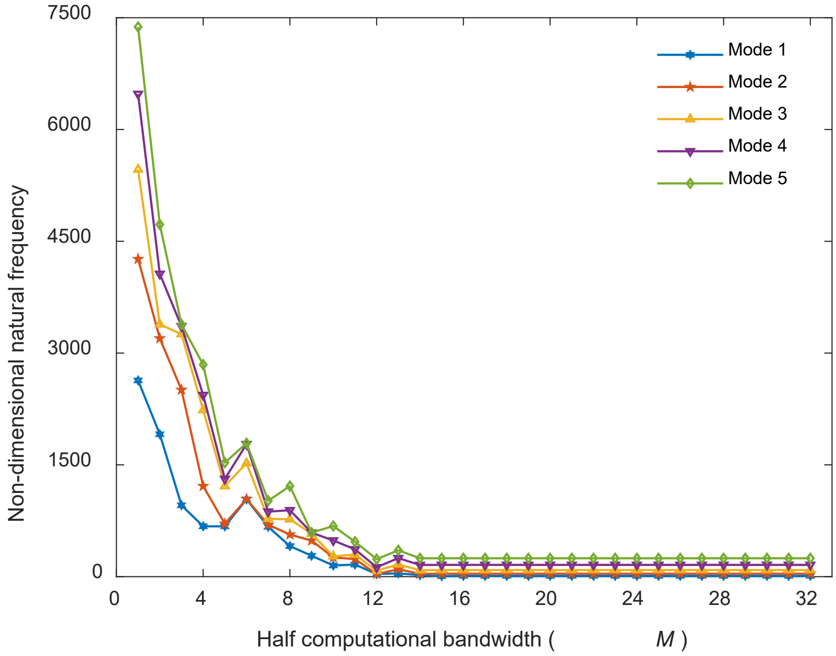


**Fig. 5.** Convergence study of first five non-dimensional frequencies for a simply supported beam

$(N = 99)$.

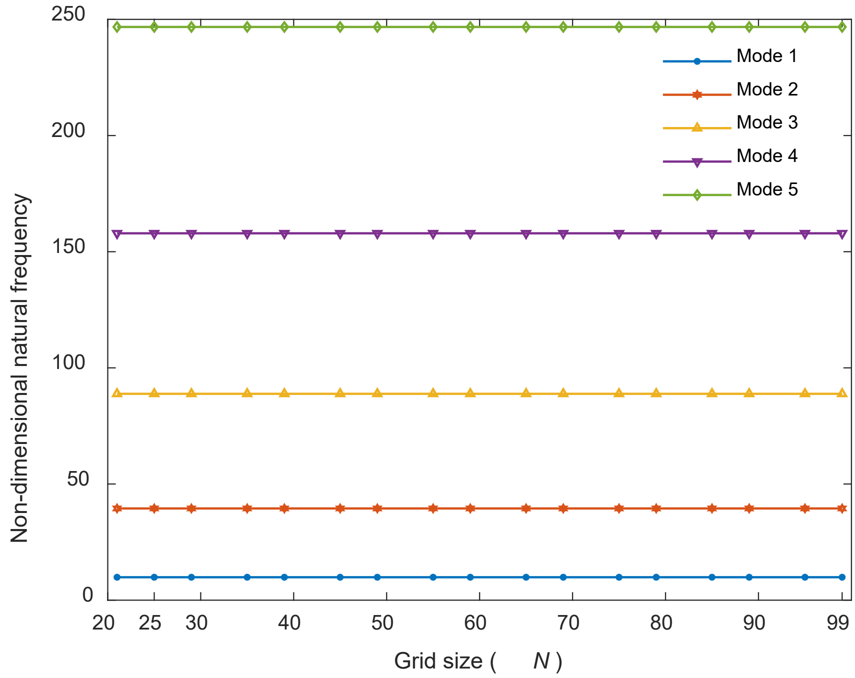


**Fig. 6.** Convergence study of non-dimensional frequency parameters for a simply supported beam

$(M = 20)$.

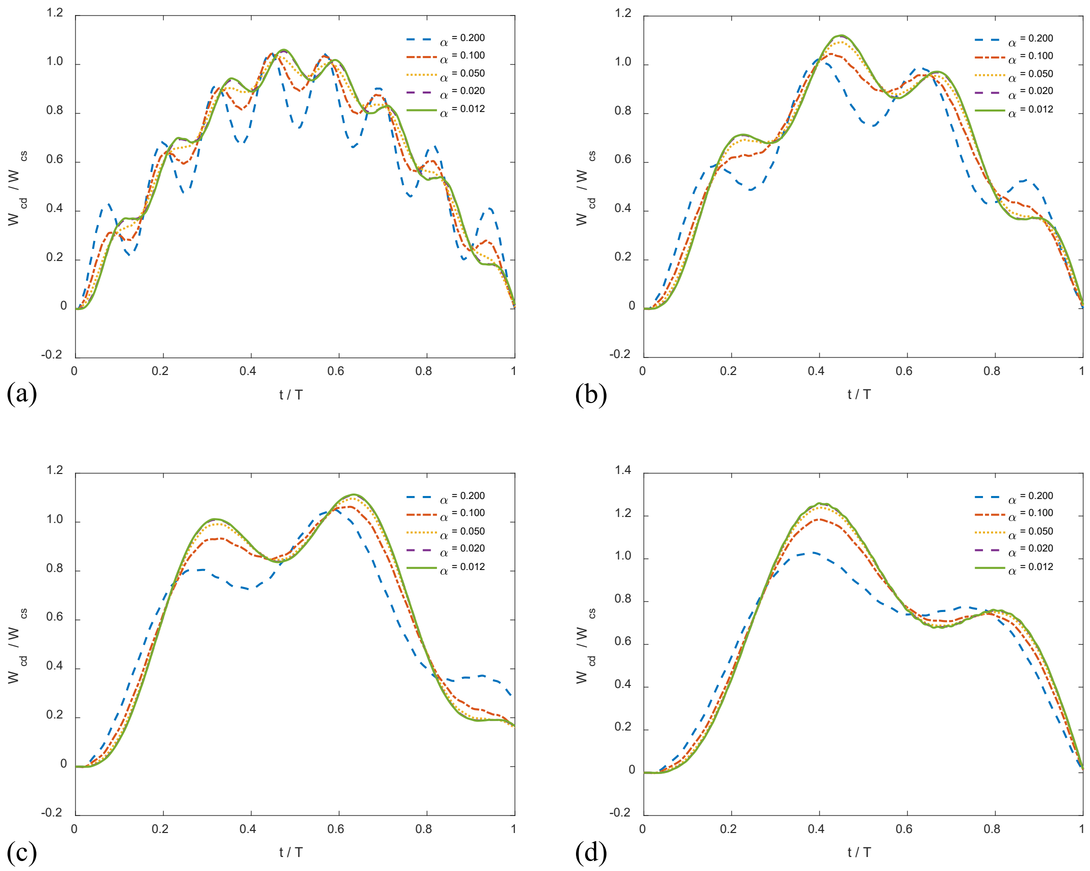


**Fig. 7.** Convergence study of the regularized parameter ($\alpha$) for the normalized central beam deflection of a simply supported beam under a moving load by DSC method ($M = 32, N = 51$): a) $v_p = 15.6\text{m/s}$, b) $v_p = 31.2\text{m/s}$, c) $v_p = 46.8\text{m/s}$ and d) $v_p = 62.4\text{m/s}$.

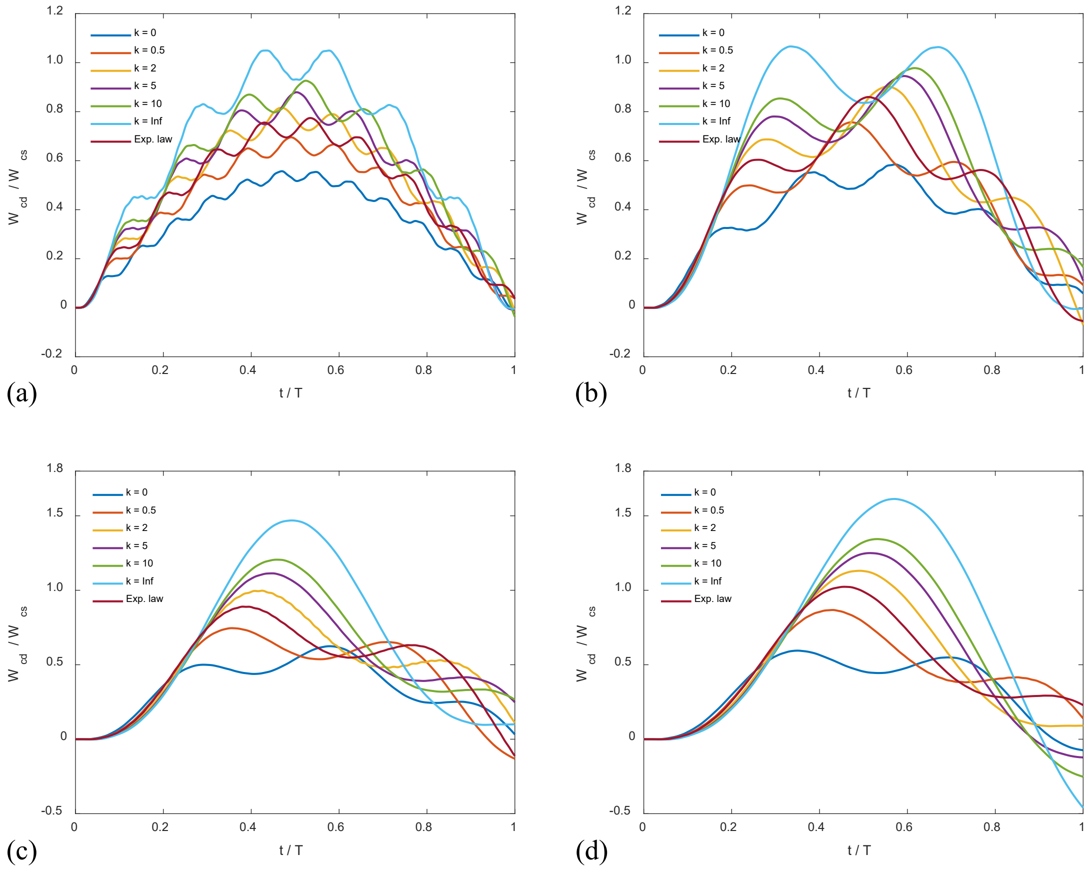


**Fig. 8.** Normalized mid-span deflection of simply supported FG beams with various material properties under a travelling load: a) $v_p = 16.3\mathrm{m/s}$, b) $v_p = 42.4\mathrm{m/s}$, c) $v_p = 65.8\mathrm{m/s}$ and d) $v_p = 84.8\mathrm{m/s}$.

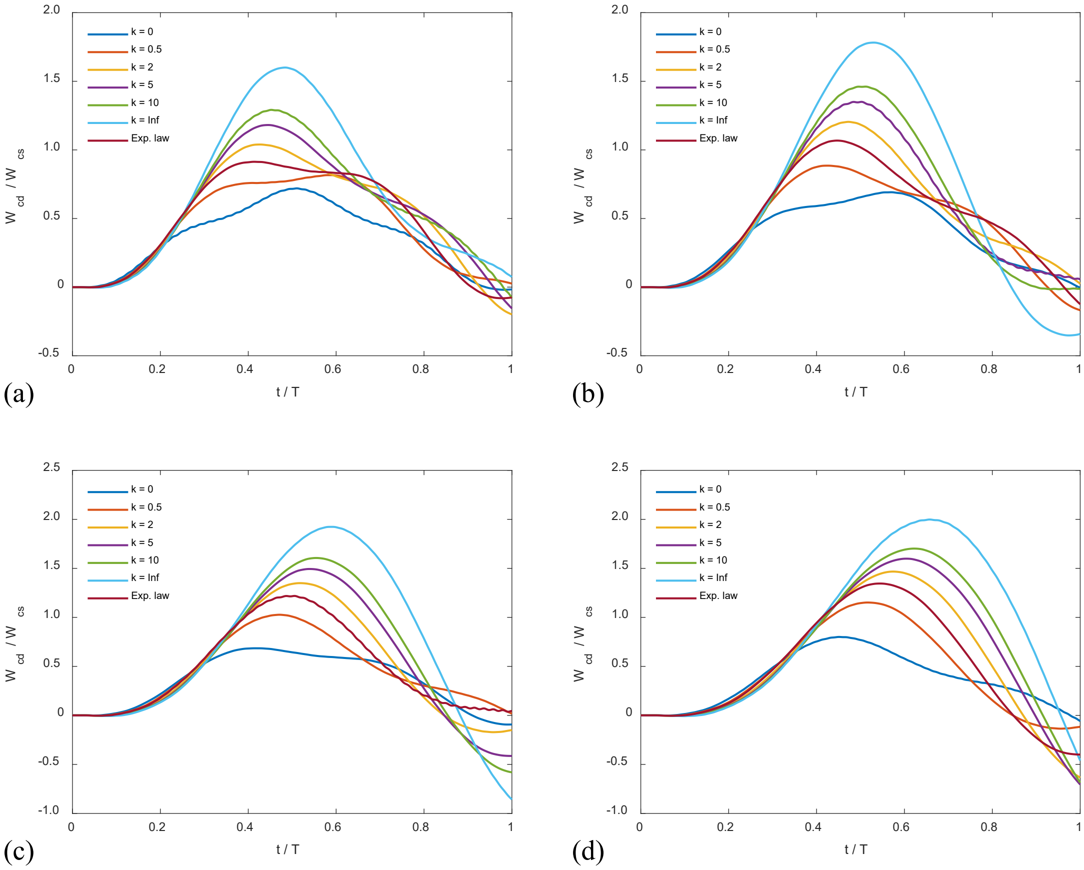


**Fig. 9.** Normalized mid-span deflection of elastically restrained FG beams ($K'$=10) with various material properties under a travelling load: a) $v_p = 108.6\text{m/s}$, b) $v_p = 130.3\text{m/s}$, c) $v_p = 156.4\text{m/s}$ and d) $v_p = 187.7\text{m/s}$.

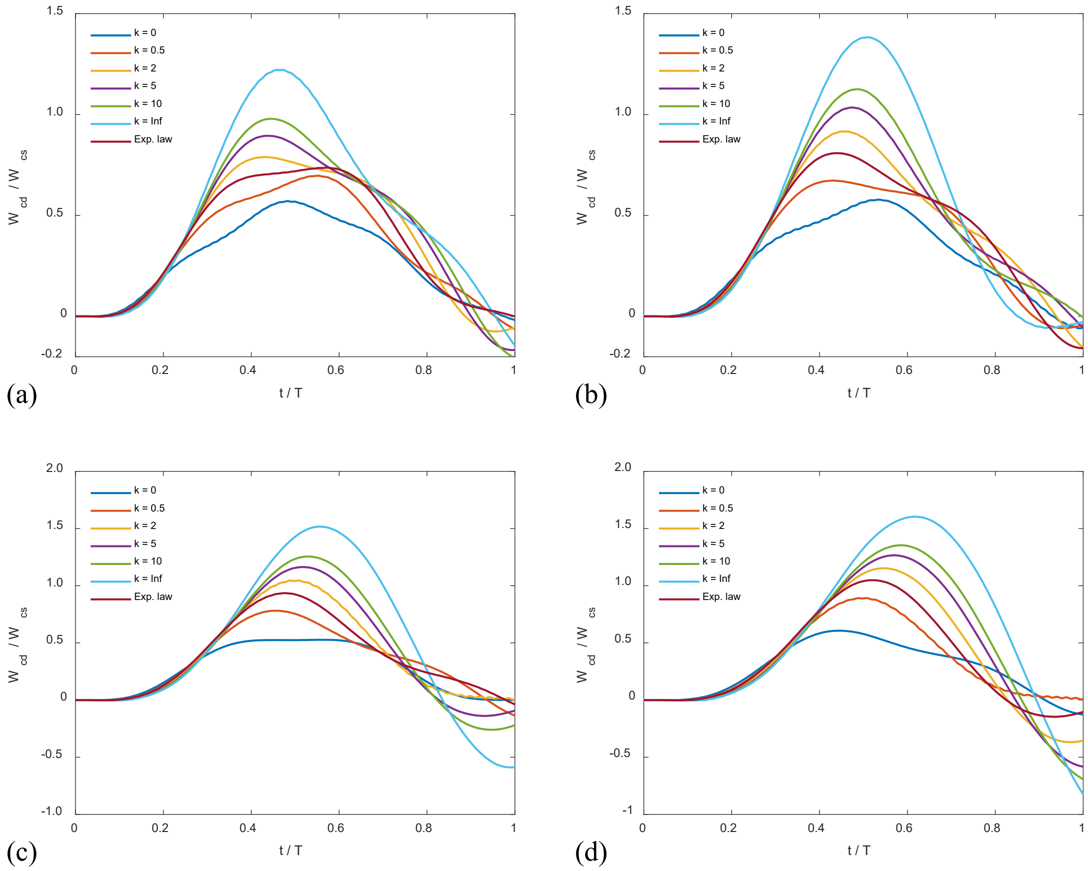


**Fig. 10.** Normalized mid-span deflection of elastically restrained FG beams ($K'$=$10^3$) with various material properties under a travelling load: a) $v_p = 108.6\text{m/s}$, b) $v_p = 130.3\text{m/s}$, c) $v_p = 156.4\text{m/s}$ and d) $v_p = 187.7\text{m/s}$.

**Table 1**

Inter-relationship coefficients ($a_m$) and static deflections ($w_{cs}$) under various boundary conditions.

| | Boundary conditions (at $\xi = 0$ or $\xi = 1$) | $a_m$ $(m = 1,2,\ldots,M)$ | $w_{cs}$ |
|---|---|---|---|
| Simple support (S) | $W(\xi) = W''(\xi) = 0$ | $-1$ | $\frac{fL^3}{48EI}$ |
| Clamped end (C) | $W(\xi) = W'(\xi) = 0$ | $1$ | $\frac{fL^3}{192EI}$ |
| Elastic support (E) | $W(\xi) = 0$<br>$EIW''(\xi) - K(s)LW'(\xi) = 0$ | $\frac{K'C_m^1 - C_m^2}{K'C_m^1 + C_m^2}$ | $\frac{fL^3}{192EI} + \frac{fL^2}{32K(s)}$ |

**Table 2**

Convergence and comparison of frequency parameters $\Omega$ for a simply supported homogeneous beam with $N = 99$.

| Half bandwidth $M$ | Mode sequence number | | | | |
|---|---|---|---|---|---|
| | $\Omega_1$ | $\Omega_2$ | $\Omega_3$ | $\Omega_4$ | $\Omega_5$ |
| 12 | 35.140 | 35.152 | 79.275 | 126.499 | 234.801 |
| 14 | 20.713 | 37.398 | 85.829 | 156.432 | 246.677 |
| 16 | 10.426 | 39.326 | 88.696 | 157.880 | 246.766 |
| 18 | 9.7816 | 39.473 | 88.823 | 157.914 | 246.741 |
| 20 | 9.8698 | 39.478 | 88.826 | 157.914 | 246.740 |
| 24 | 9.8696 | 39.478 | 88.826 | 157.914 | 246.740 |
| 28 | 9.8696 | 39.478 | 88.826 | 157.914 | 246.740 |
| 32 | 9.8696 | 39.478 | 88.826 | 157.914 | 246.740 |
| Ref. 59 | 9.8696 | 39.478 | 88.826 | 157.914 | 246.740 |

**Table 3**

First five non-dimensional natural frequencies of simply supported FG beams.

| Mode | | Power-law index ($k$) | | | | | | |
|---|---|---|---|---|---|---|---|---|
| | | 0 | 0.2 | 0.5 | 1.0 | 2 | 5 | 10 |
| $\Omega_1$ | Present | 5.4834 | 5.1019 | 4.6690 | 4.2210 | 3.8518 | 3.6675 | 3.5590 |
| | Ref. 58 | 5.4777 | - | 4.6641 | 4.2163 | 3.8472 | 3.6628 | 3.5547 |
| | Ref. 57 | 5.4777 | 5.0980 | 4.6646 | 4.2163 | 3.8472 | 3.6628 | 3.5547 |
| $\Omega_2$ | Present | 21.934 | 20.408 | 18.676 | 16.884 | 15.407 | 14.670 | 14.236 |
| | Ref. 58 | 21.845 | - | 18.599 | 16.810 | 15.333 | 14.5960 | 14.168 |
| $\Omega_3$ | Present | 49.350 | 45.917 | 42.021 | 37.989 | 34.667 | 33.007 | 32.030 |
| | Ref. 58 | 48.900 | - | 41.633 | 37.617 | 34.295 | 32.636 | 31.688 |
| $\Omega_4$ | Present | 87.734 | 81.631 | 74.7034 | 67.536 | 61.629 | 58.680 | 56.943 |
| $\Omega_5$ | Present | 137.084 | 127.548 | 116.724 | 105.525 | 96.296 | 91.687 | 88.973 |

**Table 4**

First five non-dimensional natural frequencies of clamped FG beams.

| Mode | | Power-law index ($k$) | | | | | | |
|---|---|---|---|---|---|---|---|---|
| | | 0 | 0.2 | 0.5 | 1.0 | 2 | 5 | 10 |
| $\Omega_1$ | Present | 12.430 | 11.566 | 10.584 | 9.5686 | 8.7317 | 8.3138 | 8.0677 |
| | Ref. 57 | 12.414 | 11.554 | 10.571 | 9.5554 | 8.6040 | 8.1699 | 8.0556 |
| $\Omega_2$ | Present | 34.265 | 31.881 | 29.176 | 26.376 | 24.070 | 22.918 | 22.239 |
| $\Omega_3$ | Present | 67.174 | 62.501 | 57.197 | 51.709 | 47.187 | 44.928 | 43.598 |
| $\Omega_4$ | Present | 111.044 | 103.319 | 94.551 | 85.479 | 78.004 | 74.270 | 72.072 |
| $\Omega_5$ | Present | 165.884 | 154.345 | 141.247 | 127.695 | 116.527 | 110.950 | 107.666 |

**Table 5**

Fundamental non-dimensional frequencies of elastically restrained FG beams.

| $K'$ | Power-law index ($k$) | | | | | | | |
|---|---|---|---|---|---|---|---|---|
| | 0 | 0.2 | 0.5 | 1.0 | 2 | 5 | 10 | Exp. law |
| 0 | 5.4834 | 5.1019 | 4.6690 | 4.2210 | 3.8518 | 3.6675 | 3.5589 | 3.8997 |
| $10^{-1}$ | 5.7105 | 5.3132 | 4.8624 | 4.3958 | 4.0114 | 3.8194 | 3.7063 | 4.0613 |
| $10^{1}$ | 7.1821 | 6.6825 | 6.1154 | 5.5287 | 5.0452 | 4.8037 | 4.6615 | 5.1078 |
| $10^{2}$ | 10.687 | 9.9432 | 9.0994 | 8.2263 | 7.5069 | 7.1476 | 6.9360 | 7.6003 |
| $10^{3}$ | 12.185 | 11.337 | 10.375 | 9.3798 | 8.5595 | 8.1498 | 7.9086 | 8.6659 |
| $10^{4}$ | 12.403 | 11.540 | 10.561 | 9.5479 | 8.7128 | 8.2958 | 8.0503 | 8.8212 |
| $10^{5}$ | 12.428 | 11.563 | 10.582 | 9.5665 | 8.7298 | 8.3120 | 8.0660 | 8.8384 |
| $\infty$ | 12.428 | 11.563 | 10.582 | 9.5665 | 8.7298 | 8.3120 | 8.0660 | 8.8401 |

**Table 6**

Convergence and comparison for the maximum value of the normalized mid-span displacement of a simply supported beam under a moving load ($M = 32, N = 51$).

| $v_p$ | Parameter of regularization in Dirac-delta function ($\alpha$) | | | | | | | |
|---|---|---|---|---|---|---|---|---|
| (m/s) | 0.200 | 0.100 | 0.050 | 0.020 | 0.016 | 0.012 | Ref. 37[a] | Ref. 5[b] |
| 31.20 | 1.0225 | 1.0447 | 1.0924 | 1.1171 | 1.1190 | 1.1209 | 1.1220 | 1.1216 |
| 62.40 | 1.0282 | 1.1837 | 1.2390 | 1.2556 | 1.2568 | 1.2576 | 1.2550 | 1.2585 |
| 78.00 | 1.2059 | 1.3721 | 1.4256 | 1.4410 | 1.4420 | 1.4424 | 1.4414 | 1.4434 |
| 93.60 | 1.3455 | 1.5030 | 1.5548 | 1.5715 | 1.5727 | 1.5732 | 1.5733 | 1.5742 |
| 109.2 | 1.4451 | 1.5958 | 1.6418 | 1.6563 | 1.6574 | 1.6578 | 1.6591 | 1.6590 |
| 140.2 | 1.5362 | 1.6736 | 1.7131 | 1.7243 | 1.7251 | 1.7255 | 1.7247 | 1.7263 |
| 156.0 | 1.5498 | 1.6792 | 1.7179 | 1.7296 | 1.7304 | 1.7308 | 1.7299 | 1.7315 |

[a] Based on DQM ($\alpha = 0.018, N = 51$).

[b] Analytical solutions.

**Table 7**

Convergence and comparison for the maximum value of the normalized mid-span displacement of a clamped beam under a moving load ($M = 32, N = 51$).

| $v_p$ | Parameter of regularization in Dirac-delta function ($\alpha$) | | | | | | | |
|---|---|---|---|---|---|---|---|---|
| (m/s) | 0.200 | 0.100 | 0.050 | 0.020 | 0.016 | 0.012 | Ref. 37[a] | Ref. 8[b] |
| 141.307 | 0.9404 | 1.1903 | 1.2771 | 1.3045 | 1.3064 | 1.3078 | 1.303 | 1.311 |
| 282.614 | 1.3624 | 1.5572 | 1.6168 | 1.6343 | 1.6355 | 1.6367 | 1.636 | 1.637 |
| 423.921 | 1.3540 | 1.4787 | 1.5171 | 1.5296 | 1.5305 | 1.5513 | 1.549 | 1.552 |

[a] Based on DQM ($\alpha = 0.020, N = 31$).

[b] Based on a finite element model.

**Table 8**

Maximum normalized mid-span deflection of simply supported FG beams with different material properties and moving loads.

| | Power-law index and moving speed of the load (m/s). | | | | | | |
|---|---|---|---|---|---|---|---|
| | $k = 0$<br>$v_p = 252$ | $k = 0.2$<br>$v_p = 222$ | $k = 0.5$<br>$v_p = 198$ | $k = 1.0$<br>$v_p = 179$ | $k = 2.0$<br>$v_p = 164$ | $k = \infty$<br>$v_p = 132$ | Exp. law<br>$v_p = 180$ |
| Present | 0.9321 | 1.0338 | 1.1435 | 1.2493 | 1.3365 | 1.7311 | 1.2742 |
| Ref. 28[a] | 0.9317 | 1.0333 | 1.1429 | 1.2486 | 1.3360 | 1.7302 | 1.2737 |
| Ref. 24[b] | 0.9328 | 1.0344 | 1.1444 | 1.2503 | 1.3376 | 1.7324 | 1.2754 |

[a] Based on a mixed Ritz-DQ method.

[b] Based on a Lagrange's equation and Newmark integration scheme ($n_t = 500$).

**Table 9**

Maximum normalized mid-span deflection of simply supported FG beams excited by the moving load with critical velocities.

| $v_p$ | Power-law index ($k$) | | | | | | | | |
|---|---|---|---|---|---|---|---|---|---|
| (m/s) | 0 | 0.2 | 0.5 | 1.0 | 2 | 5 | 10 | ∞ | Exp. law |
| 132 | 0.7939 | 0.9342 | 1.0784 | 1.2113 | 1.3169 | 1.4130 | 1.4934 | 1.7311 | 1.2330 |
| 164 | 0.8719 | 1.0023 | 1.1318 | 1.2466 | 1.3365 | 1.4179 | 1.4867 | 1.6893 | 1.2708 |
| 179 | 0.8951 | 1.0190 | 1.1400 | 1.2493 | 1.3319 | 1.4027 | 1.4638 | 1.6482 | 1.2742 |
| 198 | 0.9148 | 1.0296 | 1.1435 | 1.2432 | 1.3127 | 1.3705 | 1.4231 | 1.5898 | 1.2691 |
| 222 | 0.9274 | 1.0338 | 1.1364 | 1.2195 | 1.2741 | 1.3186 | 1.3652 | 1.5098 | 1.2463 |
| 252 | 0.9321 | 1.0261 | 1.1096 | 1.1743 | 1.2170 | 1.2505 | 1.2765 | 1.3469 | 1.2018 |

**Table 10**

Maximum normalized mid-span deflection of simply supported FG beams.

| $v_p$ (m/s) | | Power-law index ($k$) | | | | | | | | |
|---|---|---|---|---|---|---|---|---|---|---|
| | | 0 | 0.2 | 0.5 | 1.0 | 2 | 5 | 10 | ∞ | Exp. law |
| 20 | Present | 0.5636 | 0.6285 | 0.7012 | 0.7732 | 0.8153 | 0.8894 | 0.9526 | 1.1004 | 0.7887 |
| | Ref. 28[a] | 0.5656 | 0.6252 | 0.7048 | 0.7706 | 0.8167 | 0.8903 | 0.9466 | 1.0993 | 0.7868 |
| 40 | Present | 0.5907 | 0.6371 | 0.7421 | 0.8359 | 0.9043 | 0.9579 | 0.9993 | 1.1085 | 0.8507 |
| | Ref. 28[a] | 0.5884 | 0.6476 | 0.7511 | 0.8411 | 0.9043 | 0.9523 | 0.9893 | 1.0862 | 0.8568 |
| 60 | Present | 0.6297 | 0.6935 | 0.7326 | 0.7958 | 0.9093 | 1.0224 | 1.1103 | 1.3634 | 0.8060 |
| | Ref. 28[a] | 0.6308 | 0.6872 | 0.7175 | 0.8155 | 0.9290 | 1.0433 | 1.1332 | 1.3911 | 0.8266 |
| 80 | Present | 0.5787 | 0.6952 | 0.8354 | 0.9735 | 1.0959 | 1.2148 | 1.3084 | 1.5778 | 0.9875 |
| | Ref. 28[a] | 0.5824 | 0.7119 | 0.8538 | 0.9941 | 1.1152 | 1.2336 | 1.3275 | 1.5983 | 1.0090 |
| 100 | Present | 0.6720 | 0.8086 | 0.9560 | 1.0989 | 1.2203 | 1.3353 | 1.4264 | 1.6879 | 1.1164 |
| | Ref. 28[a] | 0.6866 | 0.8260 | 0.9732 | 1.1155 | 1.2354 | 1.3491 | 1.4395 | 1.6989 | 1.1337 |
| 125 | Present | 0.7714 | 0.9118 | 1.0585 | 1.1945 | 1.3043 | 1.4062 | 1.4869 | 1.7297 | 1.2157 |
| | Ref. 28[a] | 0.7852 | 0.9259 | 1.0715 | 1.2058 | 1.3123 | 1.4104 | 1.4912 | 1.7316 | 1.2274 |
| 150 | Present | 0.8427 | 0.9788 | 1.1148 | 1.2376 | 1.3334 | 1.4217 | 1.4966 | 1.7175 | 1.2616 |
| | Ref. 28[a] | 0.8540 | 0.9890 | 1.1223 | 1.2417 | 1.3356 | 1.4219 | 1.4949 | 1.7096 | 1.2656 |
| 175 | Present | 0.8895 | 1.0152 | 1.1381 | 1.2491 | 1.3340 | 1.4080 | 1.4707 | 1.6602 | 1.2739 |
| | Ref. 28[a] | 0.8980 | 1.0206 | 1.1409 | 1.2495 | 1.3313 | 1.4014 | 1.4616 | 1.6454 | 1.2747 |
| 200 | Present | 0.9162 | 1.0303 | 1.1435 | 1.2418 | 1.3100 | 1.3666 | 1.4187 | 1.5838 | 1.2679 |
| | Ref. 28[a] | 0.9209 | 1.0325 | 1.1428 | 1.2370 | 1.3022 | 1.3561 | 1.4038 | 1.5640 | 1.2633 |
| 225 | Present | 0.9283 | 1.0338 | 1.1346 | 1.2156 | 1.2686 | 1.3121 | 1.3579 | 1.4961 | 1.2426 |
| | Ref. 28[a] | 0.9304 | 1.0330 | 1.1293 | 1.2077 | 1.2555 | 1.2975 | 1.3413 | 1.4810 | 1.2345 |
| 250 | Present | 0.9321 | 1.0270 | 1.1117 | 1.1779 | 1.2208 | 1.2559 | 1.2845 | 1.3581 | 1.2052 |
| | Ref. 28[a] | 0.9321 | 1.0227 | 1.1042 | 1.1641 | 1.2061 | 1.2397 | 1.2754 | 1.3825 | 1.1911 |

[a] Based on a mixed Ritz-DQ method.

**Table 11**

Maximum normalized mid-span deflection of clamped FG beams.

| $v_p$ | Power-law index ($k$) | | | | | | | | |
|---|---|---|---|---|---|---|---|---|---|
| (m/s) | 0 | 0.2 | 0.5 | 1.0 | 2 | 5 | 10 | ∞ | Exp. law |
| 108.6 | 0.5691 | 0.6475 | 0.6951 | 0.7160 | 0.7867 | 0.8914 | 0.9750 | 1.2168 | 0.7352 |
| 130.3 | 0.5773 | 0.6067 | 0.6704 | 0.7954 | 0.9127 | 1.0311 | 1.1216 | 1.3776 | 0.8056 |
| 156.4 | 0.5259 | 0.6399 | 0.7780 | 0.9191 | 1.0417 | 1.1591 | 1.2506 | 1.5114 | 0.9315 |
| 187.7 | 0.6040 | 0.7407 | 0.8886 | 1.0287 | 1.1484 | 1.2614 | 1.3494 | 1.5983 | 1.0445 |

**Table 12**

Maximum normalized mid-span deflection of elastically restrained FG beams ($K' = 10$).

| $v_p$ | Power-law index ($k$) | | | | | | | | |
|---|---|---|---|---|---|---|---|---|---|
| (m/s) | 0 | 0.2 | 0.5 | 1.0 | 2 | 5 | 10 | ∞ | Exp. law |
| 108.6 | 0.7197 | 0.7845 | 0.8161 | 0.9020 | 1.0392 | 1.1813 | 1.2917 | 1.6001 | 0.9133 |
| 130.3 | 0.6915 | 0.7247 | 0.8851 | 1.0545 | 1.2043 | 1.3501 | 1.4611 | 1.7819 | 1.0678 |
| 156.4 | 0.6847 | 0.8477 | 1.0268 | 1.2013 | 1.3493 | 1.4936 | 1.6059 | 1.9234 | 1.2187 |
| 187.7 | 0.8004 | 0.9712 | 1.1516 | 1.3242 | 1.4673 | 1.5987 | 1.7018 | 1.9983 | 1.3452 |

**Table 13**

Maximum normalized mid-span deflection of elastically restrained FG beams ($K' = 10^2$).

| $v_p$ | Power-law index ($k$) | | | | | | | | |
|---|---|---|---|---|---|---|---|---|---|
| (m/s) | 0 | 0.2 | 0.5 | 1.0 | 2 | 5 | 10 | ∞ | Exp. law |
| 108.6 | 0.5880 | 0.6674 | 0.7114 | 0.7300 | 0.8147 | 0.9234 | 1.0104 | 1.2601 | 0.7496 |
| 130.3 | 0.5917 | 0.6200 | 0.6943 | 0.8241 | 0.9461 | 1.0678 | 1.1598 | 1.4249 | 0.8346 |
| 156.4 | 0.5403 | 0.6629 | 0.8065 | 0.9511 | 1.0760 | 1.1972 | 1.2920 | 1.5595 | 0.9643 |
| 187.7 | 0.6259 | 0.7676 | 0.9182 | 1.0628 | 1.1856 | 1.3014 | 1.3909 | 1.6455 | 1.0790 |

**Table 14**

Maximum normalized mid-span deflection of elastically restrained FG beams ($K' = 10^3$).

| $v_p$ | Power-law index ($k$) | | | | | | | | |
|---|---|---|---|---|---|---|---|---|---|
| (m/s) | 0 | 0.2 | 0.5 | 1.0 | 2 | 5 | 10 | ∞ | Exp. law |
| 108.6 | 0.5711 | 0.6498 | 0.6969 | 0.7176 | 0.7897 | 0.8948 | 0.9788 | 1.2214 | 0.7368 |
| 130.3 | 0.5786 | 0.6082 | 0.6730 | 0.7985 | 0.9163 | 1.0350 | 1.1257 | 1.3826 | 0.8087 |
| 156.4 | 0.5270 | 0.6423 | 0.7810 | 0.9225 | 1.0454 | 1.1631 | 1.2551 | 1.5165 | 0.9351 |
| 187.7 | 0.6063 | 0.7436 | 0.8918 | 1.0324 | 1.1524 | 1.2657 | 1.3538 | 1.6034 | 1.0482 |

**Table 15**

Maximum normalized mid-span deflection of elastically restrained FG beams ($K' = 10^4$).

| $v_p$ | Power-law index ($k$) | | | | | | | | |
|---|---|---|---|---|---|---|---|---|---|
| (m/s) | 0 | 0.2 | 0.5 | 1.0 | 2 | 5 | 10 | ∞ | Exp. law |
| 108.6 | 0.5693 | 0.6477 | 0.6952 | 0.7162 | 0.7870 | 0.8917 | 0.9754 | 1.2173 | 0.7354 |
| 130.3 | 0.5775 | 0.6069 | 0.6707 | 0.7958 | 0.9130 | 1.0315 | 1.1220 | 1.3781 | 0.8059 |
| 156.4 | 0.5260 | 0.6401 | 0.7783 | 0.9194 | 1.0421 | 1.1595 | 1.2511 | 1.5119 | 0.9319 |
| 187.7 | 0.6042 | 0.7410 | 0.8890 | 1.0291 | 1.1488 | 1.2618 | 1.3499 | 1.5989 | 1.0449 |